J. Phys. A: Math. Gen. **31** (1998) 3687–3717. Printed in the UK PII: S0305-4470(98)90026-9

Dielectric resonances of binary random networks

Th Jonckheere†§ and J M Luck‡‖

† Laboratoire Kastler-Brossel, 4, Place Jussieu, Tour 12, 1er étage, 75252 Paris cedex 05, France
‡ CEA Saclay, Service de Physique Théorique, 91191 Gif-sur-Yvette cedex, France

Received 12 December 1997, in final form 20 February 1998

Abstract. We investigate the AC conductivity of binary random impedance networks, with emphasis on its dependence on the ratio $h = \sigma_1/\sigma_0$, with σ_0 and σ_1 being the complex conductances of both phases, occurring with respective probabilities p and $1 - p$. We propose an algorithm to determine the rational h-dependence of the conductance of a finite network, in terms of its poles and of the associated residues. The poles, which lie on the negative real h-axis, are called resonances, since they show up as narrow resonances in the AC conductance of the $RL - C$ model of a metal–dielectric composite with a high quality factor Q. This approach is an extension of a previous work devoted to the dielectric resonances of isolated finite clusters. A numerical implementation of the algorithm, on the example of the square lattice, allows a detailed investigation of the resonant dielectric response of the binary model, including the p-dependence of the density of resonances and the associated spectral function, the Lifshitz behaviour of these quantities near the endpoints of the spectrum of resonances, the distribution of spacings between neighbouring resonances, and the Q-dependence of the fraction of visible resonances in the $RL - C$ model. The distribution of the local electric fields at resonance is found to be multifractal. This result is put into perspective with the giant surface-enhanced Raman scattering observed, for example, in semicontinuous metal films.

1. Introduction

Random networks of complex impedances are currently used to model electrical and optical properties of disordered inhomogeneous media. The most common situation is that of a binary composite medium, modelled by attributing a random conductance to each bond $(\boldsymbol{x}, \boldsymbol{y})$ of a lattice, according to the binary law

$$\sigma_{\boldsymbol{x},\boldsymbol{y}} = \begin{cases} \sigma_0 & \text{with probability } p \\ \sigma_1 & \text{with probability } q = 1 - p \end{cases} \tag{1.1}$$

in correspondence with the bond percolation problem (see [1] for a review).

The conductances (inverse impedances, or admittances) σ_0 and σ_1 of both phases take arbitrary frequency-dependent complex values. Hereafter we follow the notation of [2]. The dimensionless complex ratio

$$h = \frac{\sigma_1}{\sigma_0} \tag{1.2}$$

and the concentration p are the essential parameters of the model. As far as static (DC) properties are concerned, the limiting case $h = 0$ embraces the conductor–insulator mixture

§ E-mail address: thib@spectro.jussieu.fr
‖ Author to whom correspondence should be addressed. E-mail address: luck@spht.saclay.cea.fr

0305-4470/98/163687+31$19.50

($\sigma_1 = 0$) and the superconductor–conductor mixture ($\sigma_0 = \infty$). In both situations the conductivity exhibits power-law behaviour for p close to the critical concentration p_c, corresponding to the percolation threshold.

More generally, the conductivity of the binary model obeys a scaling law in the critical regions defined by $|h| \ll 1$ and $|p - p_c| \ll 1$, or equivalently $|h| \gg 1$ and $|q - p_c| \ll 1$ [1]. Frequency-dependent (AC) properties of metal–dielectric composites, such as cermets or thin films, are often investigated by means of either the $R - C$ and the $RL - C$ models [3]. In both cases the low-frequency regime corresponds to $|h| \gg 1$, and thus to critical behaviour when the metallic concentration q is near the percolation threshold.

The purpose of this work is to shed new light on the resonant behaviour of the binary model. The emphasis will be put on the analytic structure of the conductivity in the ratio h, or in the equivalent complex variable

$$\lambda = \frac{1}{1-h} = \frac{\sigma_0}{\sigma_0 - \sigma_1}. \tag{1.3}$$

For any value of the concentration p, the conductivity has singularities for h real and negative, i.e. in the range $0 \leqslant \lambda \leqslant 1$. A quantitative investigation of these singularities, and of related quantities, is the main purpose of this paper. Our aim is twofold. First, the analytic structure of the conductivity of the binary model is a classical subject, since the developments of the Bergman–Milton theory [4, 5]. The key ingredient of this formalism is the spectral function $H(p, x)$, which has only been the subject of a limited number of investigations so far [6, 7]. The present approach provides a direct accurate numerical evaluation of the spectral function of binary random networks. Second, the singularities of the conductivity have a physical interpretation in terms of dielectric resonances in the $RL-C$ model, and of the relaxation times in the transient response in the $R-C$ model. The regime of dielectric resonances has been argued to provide a natural explanation for the anomalous fluctuations of the local electric field [8], which are responsible for giant surface-enhanced Raman scattering observed, for example, in semicontinuous metal films [9].

The dielectric resonances of isolated clusters have been investigated in [2]. The situation considered there was a finite set of (metallic) bonds with conductance σ_1, embedded in an infinite (dielectric) host lattice, whose bonds have a conductance σ_0. It was shown there that the conductance of such a system is entirely characterized by a finite number of resonances. The positions λ_a of the resonances, and the associated cross sections γ_a, are expressed in terms of the eigenvalues and eigenvectors of a finite matrix $\mathbf{M}$, dictated by the geometry of the clusters. This paper is an extension of the method of [2] to an arbitrary binary network. We shall make use of an efficient algorithm, which allows for an exact determination of all the resonances of a finite sample. The set-up of this paper is as follows. In section 2, we gather definitions and results on various features of the conductivity of the binary model. Section 3 is devoted to the presentation of the algorithm. Section 4 contains a variety of numerical results, concerning especially the spectral function of the Bergman–Milton theory and the spectral density of resonances, their Lifshitz behaviour near the endpoints of the spectrum ($\lambda = 0$ and $\lambda = 1$), the number of visible resonances of a finite sample and its dependence on the quality factor Q of the $RL - C$ model, and the distribution of the local electric fields at resonance, which turns out to be multifractal.

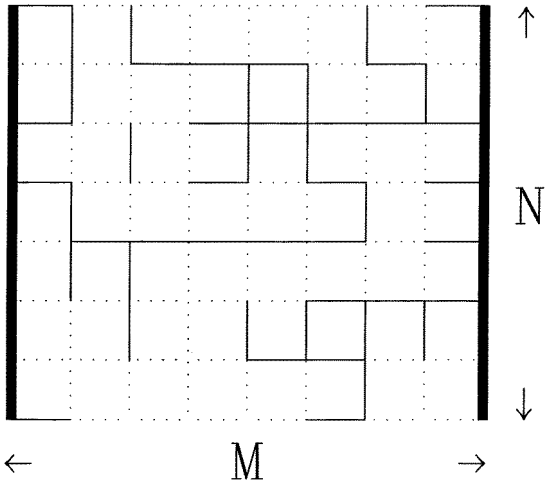

Figure 1. Schema of the binary network under consideration, with $M = N = 8$. The conductance Y is measured between the plane electrodes (bus bars). $\mathcal{P}$-bonds with conductance σ_0 are shown as full lines, $\mathcal{Q}$-bonds with conductance σ_1 are shown as dotted lines.

2. Theoretical background

2.1. Conductance and impedance of a finite network

Consider the binary model on a finite network of size $M \times N$, as shown in figure 1. This network contains $n_S = (M-1)N$ sites (nodes) and $n_B = MN+(M-1)(N-1)$ bonds (links), among which MN are horizontal (perpendicular to the electrodes), and $(M-1)(N-1)$ are vertical (parallel to the electrodes). The bonds with a conductance σ_0 are called the $\mathcal{P}$-bonds, which form the $\mathcal{P}$-set. There are $n_\mathcal{P}$ of them, among which $n_\mathcal{P}^H$ are horizontal and $n_\mathcal{P}^V$ are vertical. Similarly, the bonds with a conductance σ_1 are called the $\mathcal{Q}$-bonds, which form the $\mathcal{Q}$-set. There are $n_\mathcal{Q}$ of them, among which $n_\mathcal{Q}^H$ are horizontal and $n_\mathcal{Q}^V$ are vertical.

Let Y be the conductance (admittance) of the network, measured between the plane electrodes (bus bars) shown in figure 1, and let $Z = 1/Y$ be its impedance. These quantities are rational functions of the dimensionless complex variables h or λ. Let us anticipate that it is more convenient to use the variable λ. We have

$$Y = \frac{N\sigma_0}{M}\prod_{a=1}^{n_R}\frac{\lambda-\tilde{\lambda}_a}{\lambda-\lambda_a} = \frac{N\sigma_0}{M}\left(1-\sum_{a=1}^{n_R}\frac{\alpha_a}{\lambda-\lambda_a}\right) \tag{2.1a}$$

$$Z = \frac{M}{N\sigma_0}\prod_{a=1}^{n_R}\frac{\lambda-\lambda_a}{\lambda-\tilde{\lambda}_a} = \frac{M}{N\sigma_0}\left(1+\sum_{a=1}^{n_R}\frac{\beta_a}{\lambda-\tilde{\lambda}_a}\right). \tag{2.1b}$$

The prefactors of these expressions are the conductance and the impedance of the uniform network whose bonds have a conductance σ_0, since $\lambda = \infty$ corresponds to $\sigma_1 = \sigma_0$ (no disorder). The λ_a involved in the product expressions are the poles of the conductance and the zeros of the impedance, while the $\tilde{\lambda}_a$ are the zeros of the conductance and the poles of the impedance. The number n_R of poles and zeros depends on the configuration of the random bonds. It is bounded by the number of sites of the network: $0 \leqslant n_R \leqslant n_S$. Finally, the partial-fraction expansions involve residues α_a and β_a.

It follows from considerations on the dissipated power that Y/σ_0 is a Stieltjes function, namely its imaginary part has the sign of $\operatorname{Im} h$, or equivalently of $\operatorname{Im}\lambda$ [4, 5, 1]. This

property implies that the poles and zeros of Y and of Z alternate, according to

$$0 \leqslant \lambda_1 < \tilde{\lambda}_1 < \cdots < \lambda_{n_R} < \tilde{\lambda}_{n_R} \leqslant 1. \tag{2.2}$$

We have $\lambda_1 = 0$ if, and only if, the $\mathcal{Q}$-set is conducting, i.e. it contains at least one connected path between both electrodes. The conductance of this $\mathcal{Q}$-set then reads

$$Y_{\mathcal{Q}} = \frac{N}{M}\alpha_1\sigma_1. \tag{2.3}$$

Similarly, we have $\tilde{\lambda}_{n_R} = 1$ if, and only if, the $\mathcal{P}$-set is not conducting.

The Stieltjes property also implies that the residues α_a and β_a are positive. These two sets of residues are different from each other in general. They obey, however, a remarkable sum rule, which can be proved by expanding the conductance Y around $\lambda = \infty$, to first order in $1/\lambda$. Indeed, $1/\lambda = (\sigma_0 - \sigma_1)/\sigma_0$ is the dimensionless contrast between the conductances of both phases. As a consequence, for a given realization of the random network, up to first order in $1/\lambda$ included, the conductance reads $Y = (N/M)\overline{\sigma_H}$, where

$$\overline{\sigma_H} = \frac{n_{\mathcal{P}}^H\sigma_0 + n_{\mathcal{Q}}^H\sigma_1}{MN} = \sigma_0\left(1 - \frac{n_{\mathcal{Q}}^H}{MN\lambda}\right) \tag{2.4}$$

is the average value of the conductances of the horizontal bonds of the network. By inserting this estimate into the second expressions of equations (2.1a) (1b), we obtain the relation

$$\sum_{a=1}^{n_R}\alpha_a = \sum_{a=1}^{n_R}\beta_a = \frac{n_{\mathcal{Q}}^H}{MN}. \tag{2.5}$$

In the case of isolated finite clusters [2], the poles and zeros of the conductance form very tight doublets. We have indeed

$$\alpha_a \approx \beta_a \approx \tilde{\lambda}_a - \lambda_a \approx \frac{\gamma_a\lambda_a(1-\lambda_a)}{MN}. \tag{2.6}$$

The sum rule (2.5) then becomes

$$\sum_{a=1}^{n_R}\gamma_a\lambda_a(1-\lambda_a) = n_H \tag{2.7}$$

where n_H is the number of horizontal bonds in the clusters (perpendicular to the electrodes). This identity was not noted in [2].

2.2. $R-C$ model

The $R-C$ model, already mentioned in the introduction, is defined as follows. The $\mathcal{Q}$-set is a metallic phase, whose bonds consist of a pure resistance R, while the $\mathcal{P}$-set is a dielectric phase, whose bonds consist of a perfect capacitance C. The complex conductances at frequency $f = \omega/(2\pi)$ thus read

$$\sigma_0 = \mathrm{i}C\omega \qquad \sigma_1 = \frac{1}{R}. \tag{2.8}$$

Along the lines of [1, 2], we introduce the microscopic relaxation time

$$\tau = RC \tag{2.9}$$

so that

$$h = \frac{1}{\mathrm{i}\omega\tau} \qquad \lambda = \frac{\mathrm{i}\omega\tau}{\mathrm{i}\omega\tau - 1}. \tag{2.10}$$

We thus have $h \to \infty$ and $\lambda \to 0$ at low frequency.

The poles of the conductance Y show up as relaxation times in the transient response of the model [1]. Consider indeed the $R-C$ model on a finite network, submitted to a voltage $V(t) = V_0\theta(t)$ applied between the electrodes, with $\theta(t)$ being the Heaviside step-function. The intensity $I(t)$ across the network in the transient regime can be evaluated by means of the Fourier transformation. We thus obtain

$$I(t) = \int_{-\infty}^{+\infty} \frac{\mathrm{d}\omega}{2\pi} Y(\omega) \mathrm{e}^{\mathrm{i}\omega t} \frac{V_0}{\mathrm{i}\omega + 0}. \tag{2.11}$$

The second expression of equation (2.1*a*) for the conductance Y, with λ given in equation (2.10), yields the result

$$I(t) = \frac{NV_0}{MR} \sum_{a=1}^{n_R} \frac{\alpha_a}{(1-\lambda_a)^2} \exp\left(-\frac{t}{\tau_a}\right) \tag{2.12}$$

where the relaxation times read

$$\tau_a = \frac{1-\lambda_a}{\lambda_a}\tau. \tag{2.13}$$

If the metallic $\mathcal{Q}$-phase is conducting, we have $\lambda_1 = 0$. The term $a = 1$ in equation (2.12) yields the DC current through the network, $I_0 = NV_0\alpha_1/(MR)$, in agreement with the result (2.3).

2.3. $RL-C$ model

In the $RL-C$ model, already mentioned in the introduction, the metallic bonds of the $\mathcal{Q}$-set now consist of an inductance L in series with a weak resistance R, while the dielectric bonds of the $\mathcal{P}$-set still consist of a perfect capacitance C. The conductances at frequency $f = \omega/(2\pi)$ now read

$$\sigma_0 = \mathrm{i}C\omega \qquad \sigma_1 = \frac{1}{R + \mathrm{i}L\omega}. \tag{2.14}$$

Along the lines of [1–3], we introduce the microscopic resonance frequency

$$\omega_0 = \frac{1}{\sqrt{LC}} \tag{2.15}$$

the reduced frequency

$$y = \frac{\omega}{\omega_0} \tag{2.16}$$

and the quality factor

$$Q = \frac{1}{R}\sqrt{\frac{L}{C}} = \frac{L\omega_0}{R} = \frac{1}{RC\omega_0} \tag{2.17}$$

which is a dimensionless measure of the dissipation rate.

In the following, we shall mostly consider the case of a weak dissipation, corresponding to a large quality factor ($Q \gg 1$). We then have

$$h = \frac{1}{-y^2 + \mathrm{i}y/Q} \approx -\frac{1}{y^2} - \frac{\mathrm{i}}{y^3 Q} \qquad \lambda = \frac{y^2 - \mathrm{i}y/Q}{1 + y^2 - \mathrm{i}y/Q} \approx \frac{y^2}{1+y^2} - \frac{\mathrm{i}y}{(1+y^2)^2 Q}. \tag{2.18}$$

Note that the low-frequency regime ($y \to 0$) again corresponds to $h \to \infty$ and $\lambda \to 0$.

Since the variables h and λ have a small (negative) imaginary part, proportional to $1/Q$, the poles of the conductance Y and of the impedance Z of the network show up in the frequency dependence of these quantities as narrow resonances, respectively located at $\omega_a = \omega_0 y_a$ and $\tilde{\omega}_a = \omega_0 \tilde{y}_a$, with

$$y_a = \sqrt{\frac{\lambda_a}{1-\lambda_a}} \qquad \tilde{y}_a = \sqrt{\frac{\tilde{\lambda}_a}{1-\tilde{\lambda}_a}}. \tag{2.19}$$

We have indeed

$$Y \approx \frac{NC\omega_0}{2M} \sum_{a=1}^{n_R} \frac{\alpha_a}{(1-\lambda_a)^2} \frac{1/(2Q) - \mathrm{i}(y-y_a)}{(y-y_a)^2 + 1/(4Q^2)} \tag{2.20a}$$

$$Z \approx \frac{M}{2NC\omega_0} \sum_{a=1}^{n_R} \frac{\beta_a}{\tilde{\lambda}_a(1-\tilde{\lambda}_a)} \frac{1/(2Q) - \mathrm{i}(y-\tilde{y}_a)}{(y-\tilde{y}_a)^2 + 1/(4Q^2)}. \tag{2.20b}$$

Equation (2.20*a*) shows that the real part $\mathrm{Re}\, Y(\omega)$ of the conductance exhibits n_R narrow resonances, at $\omega_a = \omega_0 y_a$. The resonance peaks have a Lorentzian shape, with a common absolute width $\Delta\omega = \omega_0/(2Q)$. The maxima at resonance read

$$(\mathrm{Re}\, Y)_{\max} \approx \frac{N}{MR} \frac{\alpha_a}{(1-\lambda_a)^2} \tag{2.21}$$

while the area under each resonance peak is

$$\mathcal{A}_a = \int_{\omega\sim\omega_a} \mathrm{Re}\, Y(\omega)\, \mathrm{d}\omega \approx \frac{\pi N}{2ML} \frac{\alpha_a}{(1-\lambda_a)^2}. \tag{2.22}$$

A similar pattern of resonances can be observed on the real part $\mathrm{Re}\, Z(\omega)$ of the impedance (2.20*b*), with maxima at resonance and areas under resonance peaks respectively given by

$$(\mathrm{Re}\, Z)_{\max} \approx \frac{ML}{NRC} \frac{\beta_a}{\tilde{\lambda}_a(1-\tilde{\lambda}_a)} \qquad \tilde{\mathcal{A}}_a \approx \frac{\pi M}{2NC} \frac{\beta_a}{\tilde{\lambda}_a(1-\tilde{\lambda}_a)}. \tag{2.23}$$

2.4. Spectral function and density of resonances

The conductance Y of an infinitely large network drawn on any regular lattice becomes a self-averaging quantity. In other words, the conductivity

$$\Sigma(p,\lambda) = \lim_{M,N\to\infty} \frac{MY}{N} \tag{2.24}$$

is an intrinsic characteristic of the binary model, which depends on the lattice under consideration, on the concentration p, and on the complex variable h or λ. The conductivity of the binary model has been the subject of many investigations [1]. We gather below some definitions and properties which will be useful in the following.

The second expression of equation (2.1*a*) yields the Bergman–Milton integral representation [4, 5]

$$\Sigma(p,\lambda) = \sigma_0 \left(1 - \int_0^1 \frac{H(p,x)\mathrm{d}x}{\lambda - x} \right) \tag{2.25}$$

where the positive function

$$H(p,x) = \lim_{M,N\to\infty} \sum_{a=1}^{n_R} \alpha_a \delta(x-\lambda_a) \tag{2.26}$$

is called the spectral function of the binary model. In more precise terms, it is the density of a positive measure, supported by the interval $0 \leqslant x \leqslant 1$. Indeed, as a consequence of equation (2.3), the spectral function has a singular component at $x = 0$, of the form

$$H_{\mathrm{sg}}(p, x) = A(1 - p)\delta(x) \tag{2.27}$$

with the notation to be introduced in equation (2.38), whenever the $\mathcal{Q}$-set is conducting, i.e. for $1 - p = q > p_c$.

The spectral function entirely determines the conductivity $\Sigma(p, \lambda)$, by means of the integral representation (2.25). Conversely, it is given by the inverse formula

$$H(p, x) = \frac{1}{\pi}\mathrm{Im}\,\frac{\Sigma(p, x + \mathrm{i}0)}{\sigma_0}. \tag{2.28}$$

In other words, the conductivity is analytic in the complex λ-plane cut along the interval $0 \leqslant \lambda \leqslant 1$, and its discontinuity along this cut reads

$$\mathrm{Disc}\,\Sigma(p, \lambda) = 2\mathrm{i}\pi\sigma_0 H(p, \lambda). \tag{2.29}$$

The spectral function directly yields the transient intensity $I(t)$ of the $R - C$ model on a very large network, namely

$$I(t) \approx \frac{NV_0}{MR}\int_0^1 \frac{H(p, x)\,\mathrm{d}x}{(1 - x)^2}\exp\left(-\frac{x}{1 - x}\frac{t}{\tau}\right). \tag{2.30}$$

To close up, we introduce the spectral density of resonances

$$\rho(p, x) = \lim_{M,N\to\infty}\frac{1}{MN}\sum_{a=1}^{n_R}\delta(x - \lambda_a) \tag{2.31}$$

and the total density of resonances

$$\rho_R(p) = \lim_{M,N\to\infty}\frac{n_R}{MN} = \int_0^1 \rho(p, x)\,\mathrm{d}x \tag{2.32}$$

representing the mean number of resonances per site. This quantity has a non-trivial dependence on the concentration p. It will be expressed in equation (3.14) in terms of geometrical quantities of the bond percolation problem.

2.5. Homogeneity and duality

First, the conductivity of the binary model is invariant under the simultaneous interchange $p \leftrightarrow q = 1 - p$, $\sigma_0 \leftrightarrow \sigma_1$. Indeed, let $Y = \sigma_0 F(h) = \sigma_0 f(\lambda)$ be the conductance of the network G, shown in figure 1. Then the network G', obtained from G by interchanging all the bond conductances according to $\sigma_0 \leftrightarrow \sigma_1$, has a conductance $Y' = \sigma_1 F(1/h) = \sigma_1 f(1 - \lambda)$. For a large enough network, if G is typical of the concentration p, then G' is typical of the concentration $1 - p$. The conductivity, the spectral function, and the density of resonances therefore obey the following identities, on any regular lattice

$$\Sigma(p, h) = h\Sigma(1 - p, 1/h) \tag{2.33a}$$

$$\lambda\Sigma(p, \lambda) = (\lambda - 1)\Sigma(1 - p, 1 - \lambda) \tag{2.33b}$$

$$xH(p, x) = (1 - x)H(1 - p, 1 - x) \tag{2.33c}$$

$$\rho(p, x) = \rho(1 - p, 1 - x). \tag{2.33d}$$

More interestingly, the square lattice is self-dual, i.e. invariant under the geometric transformation called duality. This concept has been introduced in physics by Kramers and Wannier [10], while its consequences on random resistor networks have been explored in a

systematic way by Straley [11]. The dual $\tilde{G}$ of a planar network G has bonds which cross those of G, the conductances of any pair of crossing bonds being inverse to each other. The duality property implies that the conductance of the whole network $\tilde{G}$ reads $\tilde{Y} = 1/Y = Z$. With the same notation as above, we have $\tilde{Y} = (1/\sigma_0)\tilde{F}(1/h) = (1/\sigma_0)\tilde{f}(\lambda)$, so that $F(h)\tilde{F}(1/h) = f(\lambda)\tilde{f}(1-\lambda) = 1$. Therefore

$$\Sigma(p,\lambda)\Sigma(p,1-\lambda) = \sigma_0^2 \tag{2.34}$$

and

$$\rho(p,x) = \rho(p,1-x). \tag{2.35}$$

Because of its nonlinearity, the duality identity (2.34) for the conductivity does not yield any identity involving the spectral function $H(p,x)$ only.

The above identities can be combined with the homogeneity properties (2.33). We thus obtain that the percolation threshold is $p_c = \frac{1}{2}$, and that the conductivity and the spectral function right at this point read

$$\Sigma(\tfrac{1}{2},\lambda) = \sqrt{\sigma_0\sigma_1} = \sigma_0\sqrt{\frac{\lambda-1}{\lambda}} \qquad H(\tfrac{1}{2},x) = \frac{1}{\pi}\sqrt{\frac{1-x}{x}}. \tag{2.36}$$

Furthermore, the spectral and total densities of resonances obey the relations

$$\rho(p,x) = \rho(p,1-x) = \rho(1-p,x) = \rho(1-p,1-x) \qquad \rho_R(p) = \rho_R(1-p). \tag{2.37}$$

2.6. Critical behaviour and scaling

As mentioned in the introduction, the conductivity exhibits scaling behaviour around the percolation threshold $p = p_c$. The conductivity of the conductor–insulator mixture vanishes for $p \leqslant p_c$, while it reads

$$\Sigma(\sigma_1 = 0) = \sigma_0 A(p) \qquad (p > p_c). \tag{2.38}$$

Similarly, the conductivity of the superconductor–conductor mixture is infinite for $p \geqslant p_c$, while it reads

$$\Sigma(\sigma_0 = \infty) = \sigma_1 B(p) \qquad (p < p_c). \tag{2.39}$$

Both amplitudes $A(p)$ and $B(p)$ have a power-law behaviour for p near p_c:

$$\begin{aligned} A(p) &\approx a(p-p_c)^t \qquad (p \to p_c^+) \\ B(p) &\approx b(p_c-p)^{-s} \qquad (p \to p_c^-). \end{aligned} \tag{2.40}$$

The conductivity of the binary mixture obeys a scaling law in the critical region defined by $|h| \ll 1$ and $|p-p_c| \ll 1$, of the form [1]

$$\Sigma(p,h) \approx \sigma_0 |p-p_c|^t \Phi_\pm(h|p-p_c|^{-s-t}) \tag{2.41}$$

where the $\Phi_\pm$ are scaling functions of one complex variable, with $\pm$ referring to the sign of $p-p_c$. The homogeneity relation (2.33*a*) allows us to describe the vicinity of the other critical point, $|h| \gg 1$ and $|q-p_c| \ll 1$.

The scaling formula (2.41) reproduces the power laws (2.40) for small values of the argument of the scaling functions, as we have $a = \Phi_+(0)$, while $\Phi_-(x) \approx bx$ as $x \to 0$. On the other hand, both scaling functions have the common power-law behaviour $\Phi_\pm(x) \approx Kx^u$, with $u = t/(s+t)$, as $|x| \to \infty$ and $|\mathrm{Arg}\, x| < \pi$, hence

$$\Sigma(p_c,h) \approx K\sigma_0 h^u \approx K(\sigma_0^s\sigma_1^t)^{1/(s+t)} \tag{2.42}$$

for $|\sigma_1| \ll |\sigma_0|$, right at the percolation threshold. More generally, the power-law behaviour (2.42) holds for $h_\star \ll |h| \ll 1$, where the crossover scale $h_\star$ reads

$$h_\star \sim |p - p_c|^{s+t} \tag{2.43}$$

while the scaling laws (2.38)–(2.40) hold in the opposite regime ($|h| \ll h_\star$).

As a consequence of equation (2.28), the spectral function also obeys a scaling law of the form (2.41), namely

$$H(p, x) \approx |p - p_c|^t \, F_\pm((1 - x)|p - p_c|^{-s-t}) \tag{2.44}$$

for $1 - x \ll 1$ and $|p - p_c| \ll 1$, and a similar law around the other critical point, i.e. for $x \ll 1$ and $|q - p_c| \ll 1$. We shall come back to the scaling law (2.44) in section 2.9.

Consider now the binary model on a large but finite sample, of size $M \times N$. In the critical region, its mean conductance obeys the finite-size scaling law

$$Y \approx \sigma_0 N^{-t/\nu} \Psi((p - p_c)N^{1/\nu}, (p - p_c)h^{-1/(s+t)}, M/N) \tag{2.45}$$

where Ψ is a three-variable scaling function. As a consequence, right at the percolation threshold, the critical region extends over a range

$$\delta h \sim N^{-(s+t)/\nu}. \tag{2.46}$$

On the square lattice, the duality symmetry implies $p_c = \frac{1}{2}$, and $A(p)B(1 - p) = 1$, hence $s = t$ and $u = \frac{1}{2}$, in agreement with equation (2.36). The common numerical value of these exponents is $s/\nu = t/\nu = 0.9745 \pm 0.0015$ [12], with the exponent of the correlation length being exactly $\nu = \frac{4}{3}$, hence $s = t = 1.300$. Hence, for $p = p_c = \frac{1}{2}$, the same critical singularity simultaneously affects both endpoints of the spectrum, $\lambda = 1$ and $\lambda = 0$, corresponding respectively to $h = 0$ and $h = \infty$, again in agreement with equation (2.36).

2.7. Sum rules

The representation (2.25) of the conductivity can be expanded as the following series in inverse powers of λ

$$\Sigma(p, \lambda) = \sigma_0 \left(1 - \sum_{k=0}^{\infty} \frac{H_k(p)}{\lambda^{k+1}}\right) \tag{2.47}$$

where the coefficients

$$H_k(p) = \int_0^1 x^k H(p, x) \, \mathrm{d}x = \lim_{M,N\to\infty} \sum_{a=1}^{n_R} \alpha_a \lambda_a^k \tag{2.48}$$

are the moments of the spectral function $H(p, x)$.

As we have already noted in section 2.1, the expansion variable $1/\lambda$ is the dimensionless contrast between the conductances of both phases. As a consequence, the expansion (2.47) can be viewed as a special case of the weak-disorder expansion of the conductivity of a random network with an arbitrary narrow distribution of bond conductances [13]. The general results to sixth order derived there can be transcribed in the present case of binary disorder on the square lattice. We thus obtain the following expressions for the first six moments,

$$\begin{aligned}
&H_0(p) = q \qquad H_1(p) = \frac{pq}{2} \qquad H_2(p) = \frac{pq}{4} \\
&H_3(p) = \frac{pq}{8}(1 + pq) \qquad H_4(p) = \frac{pq}{16}(1 + 3pq + (J - 1)pq(p - q)) \\
&H_5(p) = \frac{pq}{32}(1 + (J + 5)pq + 4(J - 1)pq(p - q) - 2(2J - 3)p^2q^2)
\end{aligned} \tag{2.49}$$

with $q = 1 - p$. The number $J = J_1 = J_2 = 1.092\,958\,179$, with the notations of [13], is the only non-trivial quantity occurring in the sixth-order expansion. We have thus derived explicit sum rules for the spectral function, which agree with the expressions given in [7]. The number J, denoted there as $1 - a_5^4$, was estimated there from numerical data to be $J = 0.9 \pm 0.5$.

2.8. Effective-medium approximation

The effective-medium approximation (EMA), introduced by Bruggeman in 1935 [14], is a self-consistent approximate scheme to evaluate the conductivity of random impedance networks [15, 16, 13], which is still being very widely used [17].

In the present case of the binary model on the square lattice, the EMA prediction for the conductivity is given by

$$p\,\frac{\Sigma^{\mathrm{EMA}} - \sigma_0}{\Sigma^{\mathrm{EMA}} + \sigma_0} + (1-p)\frac{\Sigma^{\mathrm{EMA}} - \sigma_1}{\Sigma^{\mathrm{EMA}} + \sigma_1} = 0 \tag{2.50}$$

hence

$$\begin{aligned}\Sigma^{\mathrm{EMA}} &= \sigma_0 \left((p - \tfrac{1}{2})(1-h) + \sqrt{(p-\tfrac{1}{2})^2(1-h)^2 + h} \right) \\ &= \frac{\sigma_0}{\lambda} \left(p - \tfrac{1}{2} + \sqrt{(p-\tfrac{1}{2})^2 + \lambda(\lambda - 1)} \right).\end{aligned} \tag{2.51}$$

This EMA formula for the conductivity is analytic in the λ-plane cut along the interval $\lambda_{\min} \leqslant \lambda \leqslant \lambda_{\max}$, with

$$\lambda_{\min} = \tfrac{1}{2} - \sqrt{p(1-p)} \qquad \lambda_{\max} = 1 - \lambda_{\min} = \tfrac{1}{2} + \sqrt{p(1-p)}. \tag{2.52}$$

The prediction for the associated spectral function (cf equation (2.28)) reads

$$H^{\mathrm{EMA}}(p,x) = \frac{\sqrt{x(1-x) - (p-\frac{1}{2})^2}}{\pi x} = \frac{\sqrt{(\lambda_{\max} - x)(x - \lambda_{\min})}}{\pi x}. \tag{2.53}$$

The EMA formula gives a very accurate approximation to the conductivity of the binary model in generic circumstances. For instance, the $1/\lambda$-expansion of the EMA formula (2.51) gives expressions $H_k^{\mathrm{EMA}}(p)$ for the moments which only differ from the true results (2.49), starting with $H_4(p)$, by replacing J by $J^{\mathrm{EMA}} = 1$ [13]. The EMA scheme also respects the duality symmetry (2.34). The predictions (2.51), (2.53) therefore agree with the exact results (2.36) for the conductivity and the spectral function at $p = p_c = \frac{1}{2}$. The EMA also correctly predicts the equality $s = t$, but not the common value of these exponents ($s = t = 1$ instead of 1.300).

For a generic value of the concentration ($p \neq p_c$), the endpoints (2.52) are such that $0 < \lambda_{\min} < \lambda_{\max} < 1$. The support of the EMA prediction (2.53) for the spectral function thus does not extend over the whole interval $0 \leqslant \lambda \leqslant 1$. In the vicinity of the percolation threshold ($p \to p_c = \frac{1}{2}$), we have $\lambda_{\min} = 1 - \lambda_{\max} \approx (p - p_c)^2$, in agreement with the estimate (2.43) of the crossover scale $h_\star$, with $s + t = 2$.

2.9. Lifshitz tails

It has been argued [6] that the spectral function $H(p,x)$ of the true conductivity of the binary model extends over the whole allowed spectrum $0 \leqslant \lambda \leqslant 1$, for any value of the concentration p, at variance with the EMA formula (2.53).

This argument has then been put in perspective [1] with Lifshitz singularities [18–20]. These singularities are caused by the presence of very large, and thus very improbable, ordered regions in a randomly disordered system. The original example considered by Lifshitz [18] is that of the phonon spectrum of a binary harmonic alloy, consisting of light atoms, with mass m and concentration p, and heavy atoms, with mass $M > m$ and concentration $q = 1 - p$. Lifshitz has argued that the vicinity of the upper edge $\omega_{\max}$ of the phonon spectrum of the alloy is dominated by large ordered regions, almost spherical in shape, consisting only of light atoms. He thus showed that $\omega_{\max}$ coincides with the upper edge of the pure lattice consisting only of light atoms, and that the density of states of the alloy vanishes exponentially fast near $\omega_{\max}$, as

$$\rho(\omega) \sim \exp(-c|\ln p|(\omega_{\max} - \omega)^{-d/2}) \tag{2.54}$$

where c is a lattice-dependent constant, which can be evaluated exactly. Along this line of thought, it has been argued in [1] that the spectral function of the binary model has an exponentially small Lifshitz tail, extending all the way to the endpoints $\lambda = 0$ and $\lambda = 1$ of the spectrum of resonances, of the form

$$H(p, x) \sim \exp(-C(p)x^{-d/2}) \qquad (x \to 0) \tag{2.55}$$

and similarly for $x \to 1$. This expression was rather conjectural, as the determination of the relevant ordered regions was left as an open question, so that the prefactor $C(p)$ was not predicted.

Hesselbo [21] then argued that the relevant ordered regions are hairpin configurations, as shown in figure 2(a). Let Y_n be the transversal conductance of the hairpin consisting of n cells, measured between the point electrodes shown in figure 2(a), considered as an isolated network (not embedded in the square lattice). This quantity can be evaluated from the recursion relation

$$Y_n = \sigma_1 + \left(\frac{2}{\sigma_0} + \frac{1}{Y_{n-1}}\right)^{-1} \tag{2.56}$$

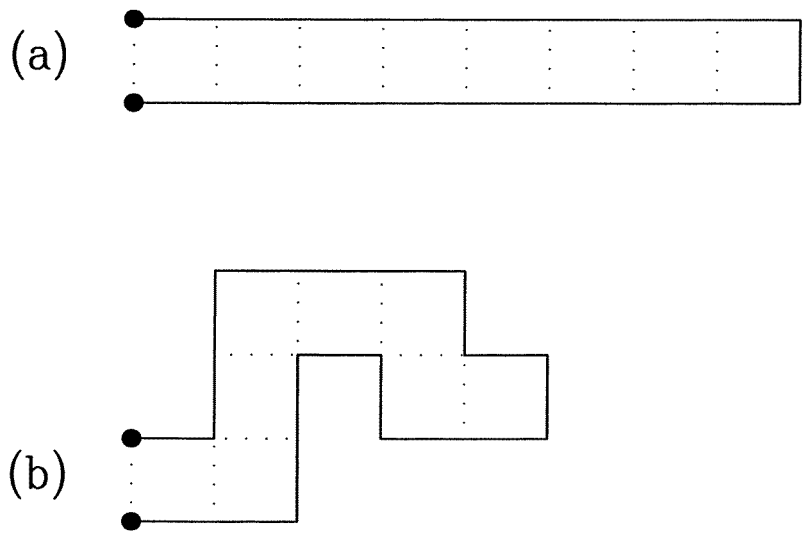

Figure 2. (a) Hairpin configuration and (b) worm-like configuration, with $n = 8$ cells. Same conventions for the bond conductances as in figure 1. The transversal conductance Y_n is measured between the point electrodes shown as large dots.

with $Y_0 = \sigma_0$. Consider first a value of h not on the negative real axis, and set

$$h = \frac{\sigma_1}{\sigma_0} = 2\sinh^2 \mu \tag{2.57}$$

with $\mathrm{Re}\,\mu > 0$ and $|\mathrm{Im}\,\mu| < \pi$. The Möbius map involved in the recursion (2.56) has two fixed points,

$$Y_\pm = \frac{\sigma_0}{2}(\mathrm{e}^{\pm 2\mu} - 1) \tag{2.58}$$

with the stable fixed point Y_+ being the transversal conductance of the infinitely long hairpin (ladder). The recursion (2.56) can be solved explicitly, along the lines of [1], by means of the variable $t_n = (Y_n - Y_-)/(Y_n - Y_+)$. We thus obtain

$$Y_n = \sigma_0 \sinh \mu \frac{3\cosh((2n+1)\mu) - \cosh((2n-1)\mu)}{3\sinh(2n\mu) - \sinh(2(n-1)\mu)}. \tag{2.59}$$

For a strong dielectric contrast ($h \to 0$), the correlation length of currents along the hairpin diverges according to $\xi = 1/(2\mu) \approx (2h)^{-1/2}$. In this regime, the conductance of long hairpins scales as

$$Y_n \approx \frac{\sigma_0}{2n} z \,\mathrm{cotanh}\, z \qquad \text{with } z = \frac{n}{\xi} = 2n\mu. \tag{2.60}$$

This scaling form of the conductance exhibits an infinite array of alternating zeros, lying at

$$\tilde{z}_a = \frac{(2a+1)\mathrm{i}\pi}{2} \qquad \text{i.e. } 1 - \tilde{\lambda}_a \approx \frac{(2a+1)^2\pi^2}{8n^2} \tag{2.61}$$

and poles, lying at

$$z_a = a\mathrm{i}\pi \qquad \text{i.e. } 1 - \lambda_a \approx \frac{a^2\pi^2}{2n^2} \tag{2.62}$$

with $a \geqslant 1$. The first zero $\tilde{\lambda}_1$, corresponding to a pole in the dual configuration, yields, according to Hesselbo, the Lifshitz behaviour of the spectral function, at least for a small enough concentration p.

It turns out that the formula (2.59) also gives the conductance of worm-like networks, such as the configuration shown in figure 2(*b*), where the square cells are put together in any random fashion, respecting the linear structure and the constraint of self-avoidance. The number of such worm-like configurations with n cells is of order $\exp(nS)$, with S being the associated configurational entropy. On the other hand, a hairpin with n cells occurs with a probability of order p^{2n}, at least for p small enough. Altogether, the first zero of equation (2.61) is expected to show up with a probability weight of order $(p^2 e^S)^n$. By eliminating the number n between the above estimates, we obtain the following analytical form for the Lifshitz tail of the density of resonances and of the spectral function

$$\rho(p,x) \sim H(p,x) \sim \exp\left(-\frac{C(p)}{\sqrt{x}}\right) \qquad (x \to 0) \tag{2.63}$$

and a similar formula for $x \to 1$. This result, with an inverse-square-root behaviour in the spectral variable x, is characteristic of Lifshitz tails in one-dimensional systems [19]. This is due to the fact that the relevant structures are linear objects. Furthermore, the identities (2.33), (2.37) imply $C(p) = C(1-p)$. The above argument also leads to a prediction for the small-p behaviour of the amplitude $C(p)$, namely

$$C(p) \approx \frac{\pi}{\sqrt{2}}\left(|\ln p| - \frac{S}{2}\right) \qquad (p \ll 1). \tag{2.64}$$

These predictions will be compared with numerical data in section 4.

The Lifshitz tail of the spectral function manifests itself in the long-time tail of the transient intensity response of the $R-C$ model. Indeed, in the regime of long times ($t \gg \tau$), equation (2.30) is dominated by the vicinity of $x = 0$, hence

$$I(t) \sim \int_0^\infty \mathrm{d}x \exp\left(-x\frac{t}{\tau} - \frac{C(p)}{\sqrt{x}}\right) \sim \exp\left\{-3\left(\frac{C(p)^2}{4}\frac{t}{\tau}\right)^{1/3}\right\}. \qquad (2.65)$$

In the critical region, the prediction (2.63) for the Lifshitz tail is compatible with the scaling law (2.44) for the spectral function, provided the amplitude $C(p)$ vanishes near the percolation threshold, according to

$$C(p) \sim |p - p_c|^{(s+t)/2}. \qquad (2.66)$$

The Lifshitz behaviour (2.63) is expected to hold only deep in the tails, for x (or $1-x$) much smaller than the crossover scale $h_\star$, defined in equation (2.43).

3. Algorithm

We now turn to the presentation of our algorithm for evaluating the rational h-dependence of the conductance of a finite binary network, such as that shown in figure 1. This approach is an extension of the method of [2]. It turns out that a very similar formalism was proposed by Straley [6] some 20 years ago, but this work has apparently not been noted since then. The conductance will be determined in the second form of equation (2.1a), namely we shall calculate first the poles λ_a of the conductance, giving the positions of the resonances, and then the associated residues α_a, giving the strengths of the resonances.

3.1. Generalities

Along the lines of [2], our starting point is the Kirchhoff equations for $V_{\boldsymbol{x}}$, the electric potential at site $\boldsymbol{x}$:

$$\sum_{\boldsymbol{y}(\boldsymbol{x})} \sigma_{\boldsymbol{x},\boldsymbol{y}}(V_{\boldsymbol{x}} - V_{\boldsymbol{y}}) = 0. \qquad (3.1)$$

There is one such equation per site $\boldsymbol{x}$ inside the network. The notation $\boldsymbol{y}(\boldsymbol{x})$ means that $\boldsymbol{y}$ is a neighbour of $\boldsymbol{x}$, i.e. there exists a bond $(\boldsymbol{x}, \boldsymbol{y})$, and the sum possibly includes sites $\boldsymbol{y}$ belonging to either electrode. Equations (3.1) have to be complemented by the boundary conditions $V_{\boldsymbol{y}} = 0$ for the sites $\boldsymbol{y}$ on the left electrode, and $V_{\boldsymbol{y}} = V_0$ for the sites $\boldsymbol{y}$ on the right electrode.

We define the topological Laplace operator Δ on the network as

$$(\Delta V)_{\boldsymbol{x}} = \sum_{\boldsymbol{y}(\boldsymbol{x})} (V_{\boldsymbol{y}} - V_{\boldsymbol{x}}) \qquad (3.2)$$

again with the convention that the sum possibly includes sites $\boldsymbol{y}$ belonging to either electrode, in which case the Dirichlet boundary condition $V_{\boldsymbol{y}} = 0$ is assumed. The operator Δ can be written as the sum $\Delta = \Delta_{\mathcal{P}} + \Delta_{\mathcal{Q}}$ of its components $\Delta_{\mathcal{P}}$ on the $\mathcal{P}$-set and $\Delta_{\mathcal{Q}}$ on the $\mathcal{Q}$-set, respectively defined as

$$(\Delta_{\mathcal{P}} V)_{\boldsymbol{x}} = \sum_{\boldsymbol{y} \in \mathcal{P}(\boldsymbol{x})} (V_{\boldsymbol{y}} - V_{\boldsymbol{x}}) \qquad (\Delta_{\mathcal{Q}} V)_{\boldsymbol{x}} = \sum_{\boldsymbol{y} \in \mathcal{Q}(\boldsymbol{x})} (V_{\boldsymbol{y}} - V_{\boldsymbol{x}}) \qquad (3.3)$$

where $\boldsymbol{y} \in \mathcal{P}(\boldsymbol{x})$ (respectively, $\boldsymbol{y} \in \mathcal{Q}(\boldsymbol{x})$) means that $(\boldsymbol{x}, \boldsymbol{y})$ is a $\mathcal{P}$-bond (respectively, a $\mathcal{Q}$-bond). We also introduce the quantities

$$\begin{cases} A_{\boldsymbol{x}}^{(L)} = 1 \text{ iff } \boldsymbol{x} \text{ is a neighbour of the left electrode} \\ A_{\boldsymbol{x}}^{(R)} = 1 \text{ iff } \boldsymbol{x} \text{ is a neighbour of the right electrode} \\ B_{\boldsymbol{x}}^{(L)} = 1 \text{ iff } \boldsymbol{x} \text{ is connected to the left electrode by a } \mathcal{Q}\text{-bond} \\ B_{\boldsymbol{x}}^{(R)} = 1 \text{ iff } \boldsymbol{x} \text{ is connected to the right electrode by a } \mathcal{Q}\text{-bond.} \end{cases} \tag{3.4}$$

With this notation, the Kirchhoff equations (3.1) read

$$\sigma_0(\Delta_{\mathcal{P}} V)_{\boldsymbol{x}} + \sigma_1(\Delta_{\mathcal{Q}} V)_{\boldsymbol{x}} + V_0(\sigma_0(A_{\boldsymbol{x}}^{(R)} - B_{\boldsymbol{x}}^{(R)}) + \sigma_1 B_{\boldsymbol{x}}^{(R)}) = 0 \tag{3.5}$$

or equivalently, in vector and matrix notation,

$$(\Delta_{\mathcal{Q}} - \lambda\Delta)\boldsymbol{V} = V_0(\lambda \boldsymbol{A}^{(R)} - \boldsymbol{B}^{(R)}). \tag{3.6}$$

This reduced form only involves the complex variable λ defined in equation (1.3). The conductance of the network is given by

$$Y = \frac{I}{V_0} \tag{3.7}$$

where the total current I flowing into the network from the left electrode reads

$$I = \sum_{\boldsymbol{x}} (\sigma_0(A_{\boldsymbol{x}}^{(L)} - B_{\boldsymbol{x}}^{(L)}) + \sigma_1 B_{\boldsymbol{x}}^{(L)}) V_{\boldsymbol{x}} \tag{3.8}$$

or equivalently, in vector notation,

$$I = \frac{\sigma_0}{\lambda}(\lambda \boldsymbol{A}^{(L)} - \boldsymbol{B}^{(L)}) \cdot \boldsymbol{V}. \tag{3.9}$$

3.2. Poles of the conductance

In analogy with [2], the poles of the conductance are the non-trivial values λ_a of λ for which the homogeneous Kirchhoff equations (3.1) with $V_0 = 0$ have a non-zero solution, namely

$$(\Delta_{\mathcal{Q}} - \lambda_a \Delta)\boldsymbol{V} = \boldsymbol{0}. \tag{3.10}$$

This is a well-posed generalized eigenvalue problem, since Δ and $\Delta_{\mathcal{Q}}$ are two real symmetric matrices, of size $n_S \times n_S$, and $(-\Delta)$ is a positive definite matrix.

It turns out that the endpoints $\lambda = 0$ or $\lambda = 1$ are in general extensively degenerate eigenvalues of equation (3.10). These eigenvalues do not correspond to resonances. Indeed, we know from section 2.1 that the conductance has no pole at $\lambda = 1$, while it has a simple pole at $\lambda = 0$ if, and only if, the $\mathcal{Q}$-phase is conducting. Let us set $\varepsilon_{\mathcal{Q}} = 1$ in this situation, $\varepsilon_{\mathcal{Q}} = 0$ else. The number of resonances then reads

$$n_R = n_S - n_0 - n_1 + \varepsilon_{\mathcal{Q}} \tag{3.11}$$

where n_0 and n_1 denote the respective multiplicities of the endpoint eigenvalues $\lambda = 0$ and $\lambda = 1$. More precisely, n_0 is the number of zero-modes of the operator $\Delta_{\mathcal{Q}}$, i.e. the dimension of its kernel. Since $\Delta_{\mathcal{Q}}$ has one zero-mode per cluster C of the $\mathcal{Q}$-phase which is disconnected from the electrodes, we have

$$n_0 = n_S - \sum_{C \subset \mathcal{Q}} (s(C) - 1 + \chi(C)). \tag{3.12}$$

In this formula, the sum runs over the clusters C of the $\mathcal{Q}$-phase, $s(C)$ denotes the number of sites of the cluster C, and the characteristic function $\chi(C)$ is unity if the cluster C overlaps

with either of the electrodes, and zero otherwise. The multiplicity n_1 of the eigenvalue $\lambda = 1$ can be expressed similarly, in terms of the clusters of the $\mathcal{P}$-phase.

In the thermodynamic limit, one can derive from equation (3.12) expressions for the fractions of eigenvalues which are condensed at $\lambda = 0$ and $\lambda = 1$. Indeed, the terms $\chi(C)$ are negligible, while the other terms can be expressed as functions of geometrical characteristics of the bond percolation problem [22], namely

$$\begin{aligned} \rho_0(p) &= \lim_{M,N\to\infty} \frac{n_0}{MN} = 1 - 2q + P(q) + n_c(q) \\ \rho_1(p) &= \lim_{M,N\to\infty} \frac{n_1}{MN} = 1 - 2p + P(p) + n_c(p) \end{aligned} \tag{3.13}$$

where $n_c(p)$ is the mean number of finite clusters per site, while $P(p)$, the percolation probability, is the probability for any given bond to belong to the infinite cluster. The latter quantity is non-vanishing only for $p > p_c$.

The density of resonances $\rho_R(p)$, defined in equation (2.32), then reads

$$\rho_R(p) = 1 - \rho_0(p) - \rho_1(p) = 1 - P(p) - P(q) - n_c(p) - n_c(q). \tag{3.14}$$

This quantity is symmetric in the exchange $p \leftrightarrow q$, in agreement with equation (2.37). For a small concentration p, the contributions to equation (3.12) of all the $\mathcal{P}$-clusters and $\mathcal{Q}$-clusters consisting of up to four bonds can be enumerated by hand. We thus obtain

$$\rho_0(p) = p^4 + \cdots \qquad \rho_1(p) = 1 - 2p + p^4 + \cdots \qquad \rho_R(p) = 2p - 2p^4 + \cdots. \tag{3.15}$$

At the percolation threshold, $\rho_R(p)$ takes its maximal value, which can be determined as follows. The percolation probability $P(p_c)$ vanishes, while $n_c(p_c)$ is known exactly [23], hence

$$\begin{aligned} &\rho_0(p_c) = \rho_1(p_c) = n_c(p_c) = \frac{3\sqrt{3} - 5}{2} = 0.098\,076 \\ &\rho_R(p_c) = 3(2 - \sqrt{3}) = 0.803\,848. \end{aligned} \tag{3.16}$$

3.3. Residues of the conductance

At any resonance corresponding to a non-trivial eigenvalue ($\lambda_a \neq 0$ and 1) of equation (3.10), the map of the electric potentials on the network is given by the components $(X_a)_{\boldsymbol{x}}$ of the associated right eigenvector $\boldsymbol{X}_a$. Since equation (3.10) is symmetric, the $\boldsymbol{X}_a$ are simultaneously its left and right eigenvectors:

$$\boldsymbol{X}_a^t(\Delta_{\mathcal{Q}} - \lambda_a \Delta) = \boldsymbol{0} \qquad (\Delta_{\mathcal{Q}} - \lambda_a \Delta)\boldsymbol{X}_a = \boldsymbol{0} \tag{3.17}$$

with the row vector $\boldsymbol{X}^t$ being the transpose of the column vector $\boldsymbol{X}$. The n_S eigenvectors $\{\boldsymbol{X}_a\}$ form a basis. They are orthogonal to each other with respect to the metric $(-\Delta)$, namely $\boldsymbol{X}_a^t(-\Delta)\boldsymbol{X}_b = 0$ for $a \neq b$. We normalize them as

$$\boldsymbol{X}_a^t(-\Delta)\boldsymbol{X}_b = \delta_{a,b}. \tag{3.18}$$

The squared norm of the eigenvector $\boldsymbol{X}_a$ reads

$$\boldsymbol{X}_a^t(-\Delta)\boldsymbol{X}_a = \sum_{(\boldsymbol{x},\boldsymbol{y})} E_{\boldsymbol{x},\boldsymbol{y}}^2 = 1 \tag{3.19}$$

where

$$E_{\boldsymbol{x},\boldsymbol{y}} = (X_a)_{\boldsymbol{x}} - (X_a)_{\boldsymbol{y}} \tag{3.20}$$

is the local electric field on the bond $(\boldsymbol{x}, \boldsymbol{y})$.

The solution $\boldsymbol{V}$ to the inhomogeneous Kirchhoff equations (3.1), (3.6) can be obtained in terms of the eigenvectors $\boldsymbol{X}_a$. Indeed, let us expand $\boldsymbol{V}$ on the basis of the $\boldsymbol{X}_a$:

$$\boldsymbol{V} = \sum_{a=1}^{n_S} c_a(\lambda)\boldsymbol{X}_a. \tag{3.21}$$

By inserting this expansion into equation (3.6), and taking the scalar product of that equation with the row vector $\boldsymbol{X}_b^t$, we readily obtain the amplitude $c_b(\lambda)$ in the form

$$c_b(\lambda) = V_0 \frac{(\lambda \boldsymbol{A}^{(R)} - \boldsymbol{B}^{(R)}) \cdot \boldsymbol{X}_b}{\lambda - \lambda_b}. \tag{3.22}$$

Finally, by inserting this result into equations (3.9), (3.7), we obtain the following formula for the residues $\alpha_a \geqslant 0$ of the conductance at its non-trivial poles ($\lambda_a \neq 0$ and 1)

$$\alpha_a = -\frac{M}{N\lambda_a}((\lambda_a \boldsymbol{A}^{(L)} - \boldsymbol{B}^{(L)}) \cdot \boldsymbol{X}_a)((\lambda_a \boldsymbol{A}^{(R)} - \boldsymbol{B}^{(R)}) \cdot \boldsymbol{X}_a). \tag{3.23}$$

As recalled in the beginning of section 3.1, the conductance also exhibits a simple pole at $\lambda = 0$, if the $\mathcal{Q}$-phase is conducting. The corresponding residue α_1, which yields the conductance of the $\mathcal{Q}$-phase by means of equation (2.3), is not directly given by equation (3.23). It can, however, be determined from the other ones $(\alpha_2, \ldots, \alpha_{n_R})$, by using the sum rule (2.5).

4. Numerical results

We have shown in section 3 that the full rational λ-dependence of the conductance of a finite binary network can be expressed in terms of the generalized eigenvalues and eigenvectors of equation (3.10). We have implemented this algorithm numerically, using the IMSL routine EIGZS, in order to obtain numerical data concerning several quantities of interest, which will be discussed successively throughout this section. The CPU time for solving the spectral problem for each sample grows rapidly with the system size, proportionally to n_S^3, i.e. to N^6 for a square sample of size $N \times N$.

The optimal use of our algorithm therefore consists in obtaining good statistics on samples of moderate sizes. We have commonly used sample sizes such as $N = 16$ or $N = 20$, and a statistical ensemble of several times 10^4 samples, having some 10^7 random bond conductances in total, a good enough statistics to obtain very accurate data. No observable systematic finite-size effects have been found, even in the critical regions ($p \to p_c$ and $\lambda \to 0$ or $\lambda \to 1$). This observation is in agreement with the argument, given at the end of section 4.1, showing that the critical regions are indeed very small in the variable λ.

4.1. Density of resonances and spectral function

We have evaluated the spectral density of resonances $\rho(p, x)$ and the spectral function $H(p, x)$, by means of their respective definitions (2.31) and (2.26). The spectral function, which plays a central role in the Bergman–Milton formalism [4, 5], had only been the subject of a limited amount of work. In [7] it has been extracted from the imaginary part of the conductance, measured at a small but finite distance ϵ from the negative real h-axis. The present method yields a direct measurement of the spectral function, avoiding especially any contamination from the delta-function at $x = 0$ (see equation (2.27)), which can be discarded in an exact way.

Figures 3 and 4 respectively show histogram plots of $\rho(p,x)$ and $xH(p,x)$, for values of the concentration p ranging from 0.05 to 0.5. Indeed, the symmetry relations (2.33), (2.37) allow us to restrict our attention to $p \leqslant p_c = \frac{1}{2}$. Each plot contain the accumulated data of an ensemble of over 20 000 configurations of a network of size $N = 16 \times 16$, corresponding to 10^7 random bonds in total. The density of resonances $\rho(p,x)$ exhibits the expected symmetry (2.37) under the transformation $x \leftrightarrow 1-x$ within a good accuracy, for all values of p. This demonstrates that we have used a large enough statistical ensemble of random networks. The product $xH(p,x)$ does not possess such a symmetry (except for $p = p_c = \frac{1}{2}$), while the EMA prediction (2.53), shown as a semicircle in figure 4, is symmetric under $x \leftrightarrow 1-x$. Both $\rho(p,x)$ and $xH(p,x)$ exhibit a rich structure, down to the scale of the resolution (each plot contains 100 bins). It will be demonstrated more clearly in section 4.2 that they are non-vanishing over the whole allowed spectrum ($0 \leqslant x \leqslant 1$).

For a small enough concentration, the most salient structures in $\rho(p,x)$ and $H(p,x)$ can be predicted from the analysis of the resonances of isolated finite clusters. For consistency with [2], we shall consider the regime $q = 1 - p \to 0$. To leading order in q, the relevant configuration consists of one isolated $\mathcal{Q}$-bond embedded in a host lattice consisting of $\mathcal{P}$-bonds. This one-bond cluster, shown as configuration A in figure 5, has one single resonance, at $\lambda = \lambda_{A1} = \frac{1}{2}$, yielding the observed leading peak in $\rho(p,x)$ and $xH(p,x)$. This one-bond cluster has two possible orientations, but only the horizontal case yields a non-vanishing residue [2], to leading order as $q \to 0$. The spectral function, the density of resonances, and the mean number of resonances therefore behave as

$$H(p,x) \approx p\delta(x-\tfrac{1}{2}) \qquad \rho(p,x) \approx 2p\delta(x-\tfrac{1}{2}) \qquad (p \to 0) \tag{4.1}$$

in agreement with the sum rules (2.49) and with equation (3.15), to leading order in p. To second order in p, $\rho(p,x)$ and $H(p,x)$ consist of a countable infinity of discrete components (delta-functions), corresponding to the resonances of configurations consisting of two bonds, in arbitrary relative position and orientation [2], and so on. The most salient subleading peaks have been marked in figures 3 and 4 (broken verticals) by some of the resonances of the two- and three-bond configurations shown in figure 5. The configurations A, B, and E are self-dual, while (C,D) and (F,G) form dual pairs. The resonances of these clusters, determined exactly along the lines of [2], are given in table 1.

Right at the percolation threshold ($p = p_c = \frac{1}{2}$), the data for the spectral function (figure 4(*e*)) agree with the exact analytical result (2.36), which coincides with the EMA prediction. The accuracy of this agreement provides another check of the quality of the numerical simulations. The density of resonances remains a non-trivial function $\rho(p_c,x)$ at the percolation threshold (figure 3(*e*)). Integrating the data of this figure leads to the estimate $\rho_R(p_c) \approx 0.80$, again in good agreement with the exact result (3.16). It is worth noting that the data shown in figures 3(*e*) and 4(*e*) are practically not affected by the critical singularities at the endpoints of the spectrum. Indeed, the size of the critical region, given by equation (2.46), can be estimated to be a few times 10^{-3}, i.e. smaller than the width of the first or last bin.

As the concentration varies from $p = 0$ to $p = p_c = \frac{1}{2}$, the profiles of the density of resonances and of the spectral function deform in a progressive way. They become smoother and smoother, with their maxima moving in a continuous way. The broken verticals are shown as guides for the eye on all plots of figures 3 and 4, although they only label the most salient structures for a small enough concentration. The spectral function also becomes progressively better in agreement with the EMA prediction.

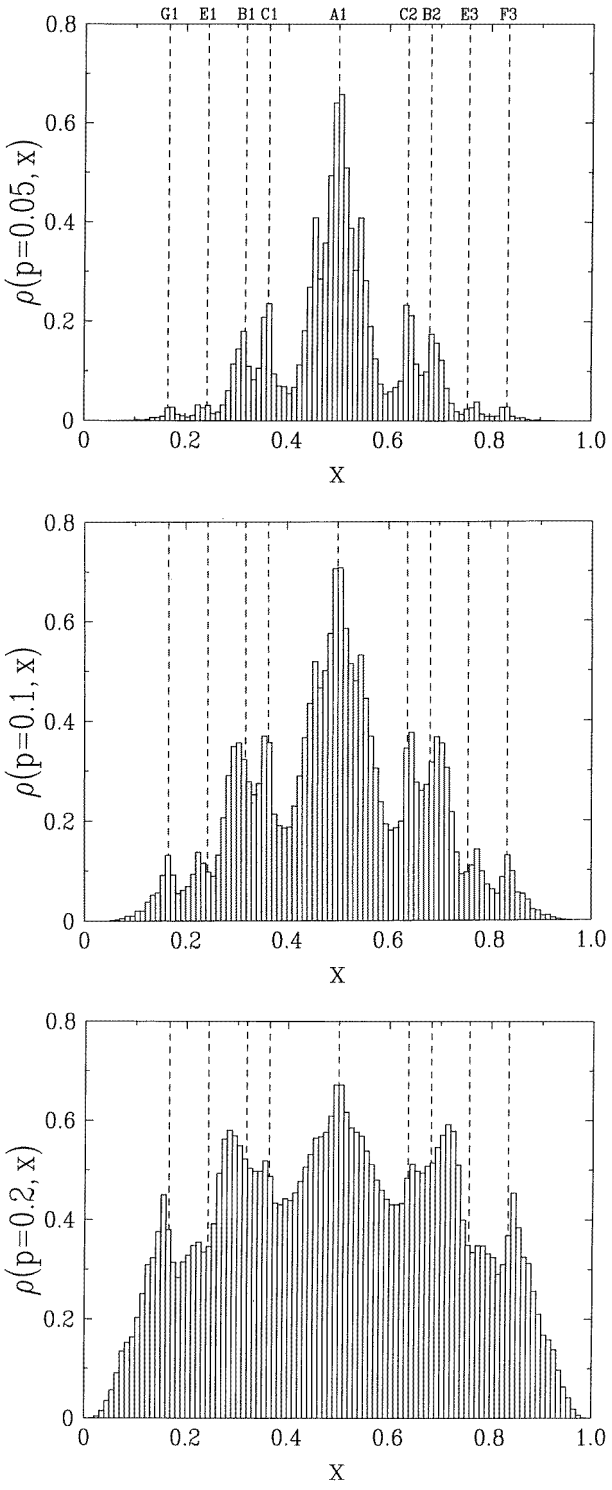

Figure 3. Histogram plot of the spectral density of resonances $\rho(p, x)$, for (*a*) $p = 0.05$, (*b*) $p = 0.1$, (*c*) $p = 0.2$, (*d*) $p = 0.3$, (*e*) $p = 0.5$. The broken verticals show some of the resonances, listed in table 1, of the configurations made of one to three bonds, shown in figure 5.

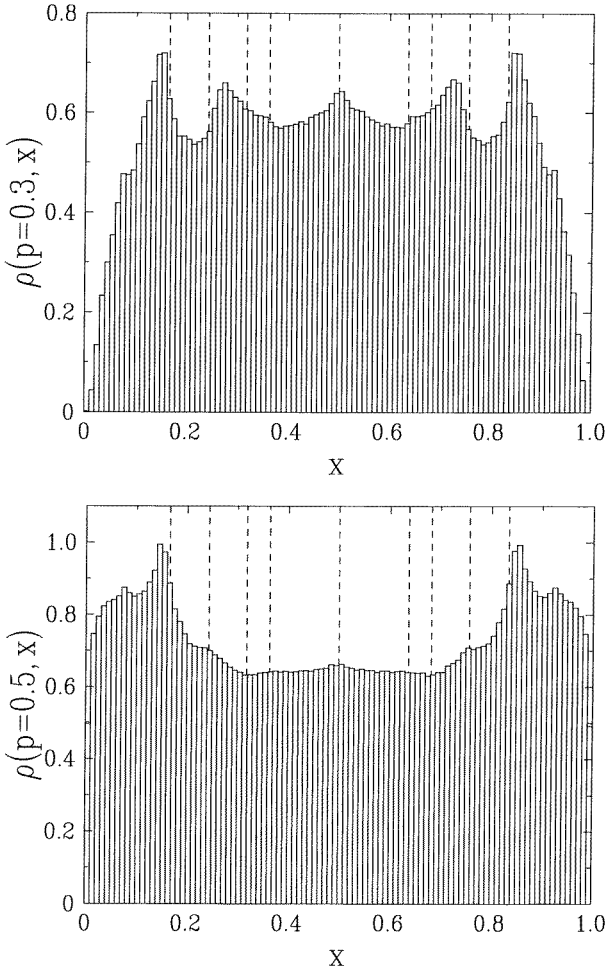

Figure 3. (Continued)

4.2. Lifshitz tails

We have also investigated the behaviour of the density of resonances near the endpoints $x = 0$ and $x = 1$, in order to check the prediction (2.63) of the Lifshitz tail. We have chosen to investigate the density of resonances $\rho(p, x)$, rather than the spectral function, because $\rho(p, x)$ can be expected on general grounds to exhibit a clearer signal, in analogy with the one-dimensional situation [19]. Furthermore, the statistics can be doubled by using the symmetry relations (2.37), and each sample requires less CPU time, since the calculation of the eigenvectors $\boldsymbol{X}_a$ is not required for $\rho(p, x)$.

Figure 6 shows a logarithmic plot of the integrated spectral density of resonances

$$\rho_{\text{int}}(p, x) = \int_0^x \rho(p, y)\,\mathrm{d}y \tag{4.2}$$

against $x^{-1/2}$, for a concentration $p = 0.1$. The data correspond to over 103 000 samples of size $N = 16 \times 16$, i.e. to 5×10^7 random bonds. The range of the plotted data corresponds to $x \leqslant \lambda_{\min}$ and $\lambda_{\max} \leqslant x \leqslant 1$, with $\lambda_{\min}$ and $\lambda_{\max}$ being the endpoints (2.52) of the EMA

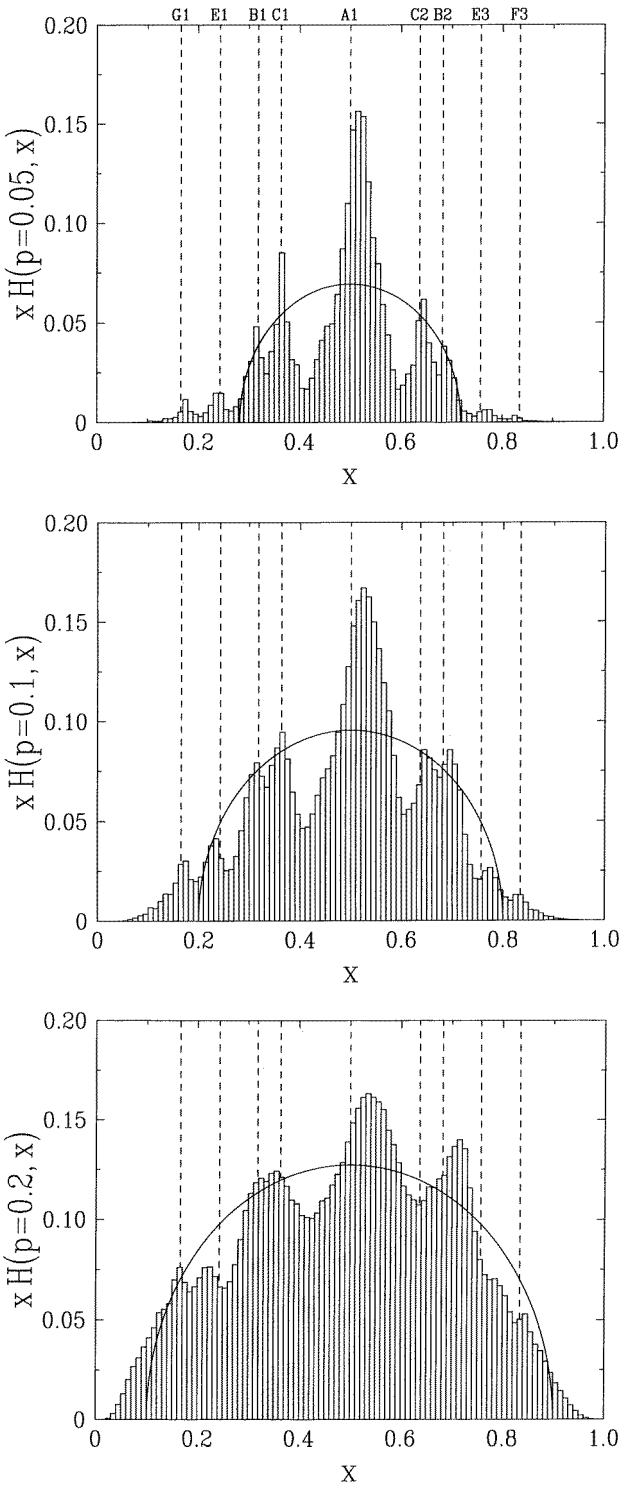

Figure 4. Histogram plot of $xH(p,x)$, with $H(p,x)$ being the spectral function of the conductivity, for (*a*) $p = 0.05$, (*b*) $p = 0.1$, (*c*) $p = 0.2$, (*d*) $p = 0.3$, (*e*) $p = 0.5$. Semicircles show the EMA prediction (2.53). Broken verticals as in figure 3.

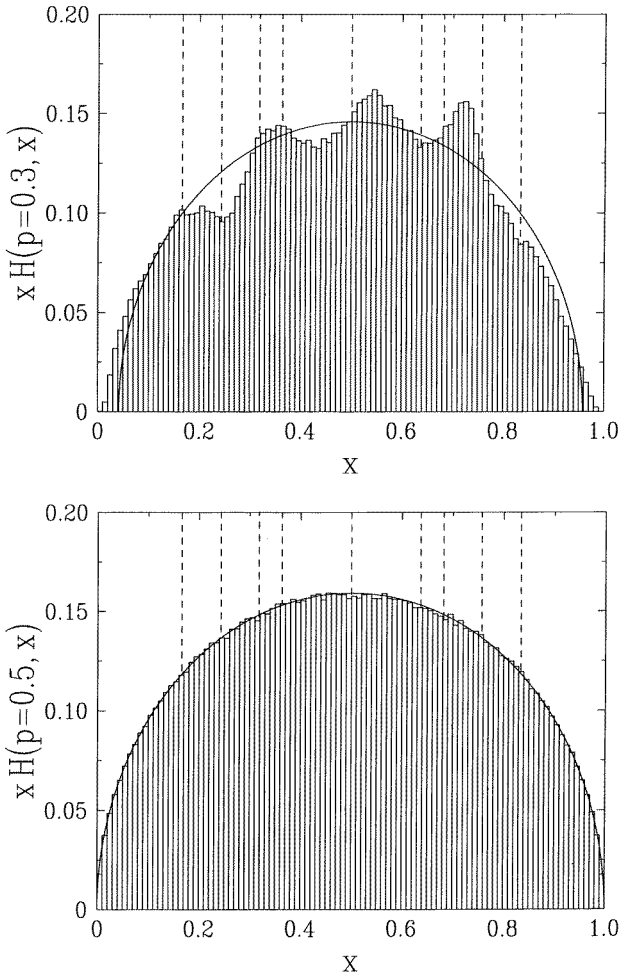

Figure 4. (Continued)

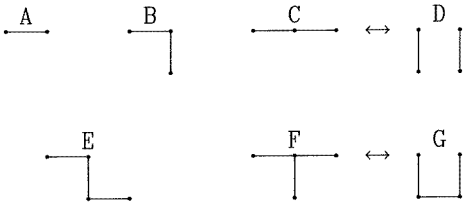

Figure 5. Configurations made of one to three bonds, whose resonances are listed in table 1, and used to label the most salient peaks in figures 3 and 4, for p small enough.

prediction for the spectral function. Indeed, the Lifshitz behaviour is expected to manifest itself mostly out of the 'bulk' of the spectrum, the latter being conveniently defined as the support of the EMA formula [20]. A linear behaviour is clearly observed, confirming the analytical form (2.63) of the Lifshitz tail. A further qualitative confirmation of Hesselbo's argument on the Lifshitz behaviour is as follows. The data of figure 6 exhibit oscillations

Table 1. Location of the resonances of some configurations consisting of one to three bonds, shown in figure 5, and used to label the most salient peaks in figures 3 and 4, for p small enough.

Configuration	Resonances
A	$\lambda_{A1} = \frac{1}{2} = 0.500\,000$
B	$\lambda_{B1} = 1/\pi = 0.318\,310$ $\lambda_{B2} = 1 - 1/\pi = 0.681\,690$
C	$\lambda_{C1} = 1 - 2/\pi = 0.363\,380$ $\lambda_{C2} = 2/\pi = 0.636\,620$
D	$\lambda_{D1} = \lambda_{C1}$ $\lambda_{D2} = \lambda_{C2}$
E	$\lambda_{E1} = \frac{1}{2} - \sqrt{2}(\frac{1}{2} - 1/\pi) = 0.243\,051$ $\lambda_{E2} = \lambda_{A1}$ $\lambda_{E3} = \frac{1}{2} + \sqrt{2}(\frac{1}{2} - 1/\pi) = 0.756\,949$
F	$\lambda_{F1} = \frac{1}{4} + 1/\pi - w/4 = 0.302\,436$ $\lambda_{F2} = \lambda_{C1}$ $\lambda_{F3} = \frac{1}{4} + 1/\pi + w/4 = 0.834\,184$
G	$\lambda_{G1} = \frac{3}{4} - 1/\pi - w/4 = 0.165\,816$ $\lambda_{G2} = \lambda_{C2}$ $\lambda_{G3} = \frac{3}{4} - 1/\pi + w/4 = 0.697\,564$
	$w = \sqrt{9 - 40/\pi + 48/\pi^2}$

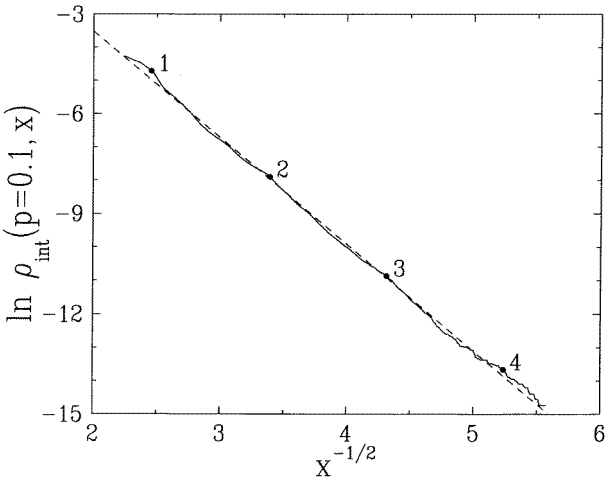

Figure 6. Logarithmic plot of the integrated density of resonances $\rho_{\rm int}(p, x)$, against $x^{-1/2}$, for a concentration $p = 0.1$. The slope of the least-squares fit yields the amplitude $C(p = 0.1) \approx 3.19$. Numbers label the lowest resonances of hairpin structures, as explained in the text.

around the fitted straight line, and the top of each of the most prominent of these oscillations corresponds, with a good accuracy, to the lowest resonance of the hairpin structures shown

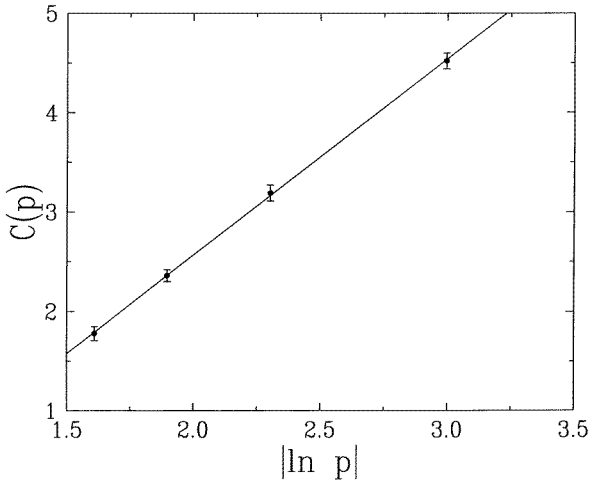

Figure 7. Plot of the measured amplitude $C(p)$ of the Lifshitz tail, against $|\ln p|$. The fitted straight line is discussed in the text.

in figure 2(a), embedded in the square lattice, with $n = 1$ to 4 cells. The case $n = 1$ corresponds to configuration G of figure 5, with its lowest resonance λ_{G1}.

From a quantitative viewpoint, the slope of the fitted straight line in figure 6 yields $C(p = 0.1) \approx 3.19$. The amplitude $C(p)$ has been similarly measured for $p = 0.05$, 0.15, and 0.2. The results are plotted in figure 7 against $|\ln p|$. The data fit nicely to the straight line $C(p) \approx 1.98|\ln p| - 1.39$, to be compared with the analytical prediction (2.64). The slope 1.98 is some 10% smaller than the analytical value $\pi/\sqrt{2} = 2.2214$. The intercept yields the estimate $S \approx 1.40$ for the configurational entropy per cell, a significantly larger value than the entropy of self-avoiding walks on the square lattice, $S_{SAW} = \ln \mu_{SAW} = 0.970$ [24]. These observations suggest that other types of linear extended structures, besides the worm-like ones identified in the framework of Hesselbo's argument, may contribute to the Lifshitz behaviour of the conductivity.

4.3. Distribution of spacings between resonances

The distribution of spacings between successive energy levels has been extensively investigated in a variety of quantum systems, ranging from nuclei to billiards [25]. Generic spectra belong to three universality classes of level spacing distributions, according to their symmetry properties, in correspondence with the classical ensembles of real symmetric, Hermitian, and symplectic random matrices [26], respectively called the Gaussian orthogonal ensemble (GOE), the Gaussian unitary ensemble (GUE), and the Gaussian symplectic ensemble (GSE).

We have investigated the distribution of spacings between successive resonances in the range

$$p = p_c = \tfrac{1}{2} \qquad \tfrac{1}{4} \leqslant x \leqslant \tfrac{3}{4} \tag{4.3}$$

where the spectral density of resonances is very flat, i.e. very close to being a constant, $\overline{\rho} = 0.658$ (see figure 3(e)). The range (4.3) can be considered as fully generic, although the concentration assumes its critical value p_c, since the critical singularities only influence very small regions around the endpoints $x = 0$ or $x = 1$, as explained in section 4.1.

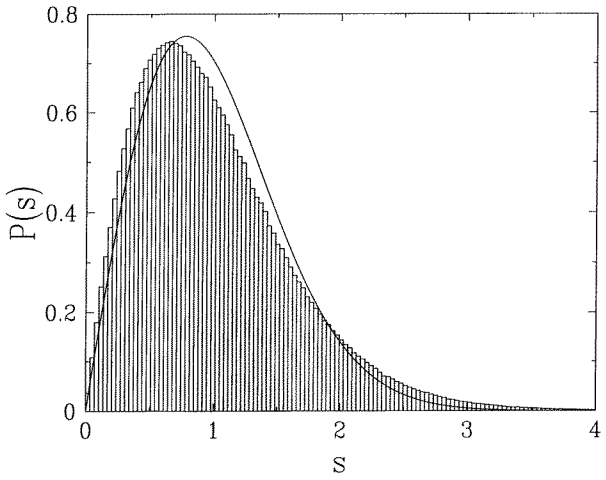

Figure 8. Histogram plot of the distribution $P(s)$ of normalized spacings between neighbouring resonances, measured in the range (4.3). The full curve shows the GOE prediction.

For a finite network of size $N \times N$, the mean spacing between two successive resonances is approximately $\lambda_{a+1} - \lambda_a \approx 1/(\overline{\rho} N^2)$. We thus define the reduced spacings

$$s_a = \overline{\rho} N^2 (\lambda_{a+1} - \lambda_a). \tag{4.4}$$

Figure 8 shows a histogram plot of the distribution $P(s)$ of the spacings s_a, obtained from an ensemble of networks of size 20×20 having 10^7 random bonds in the range (4.3) in total. This distribution obeys by construction $\int_0^\infty P(s)\mathrm{d}s = \int_0^\infty s P(s)\mathrm{d}s = 1$.

Since the generalized eigenvalue problem (3.10) involves two real symmetric matrices, Δ and Δ_Q, the natural universality class with which the data for $P(s)$ should be compared is the GOE. The law $P_{\mathrm{GOE}}(s)$ [26] is shown as a full curve in figure 8. The data share characteristic qualitative features of the GOE spacing distribution, including a linear repulsion at short spacings, i.e. $P(s) \sim s$ for $s \ll 1$, and a fast fall-off at large spacings. There is, however, a small but significant quantitative difference between the data in the range (4.3) and the GOE prediction.

4.4. Number of visible resonances

We now turn to the number of visible resonances of the $RL-C$ model on a finite network. A resonance is said to be visible if it corresponds to a true maximum in the frequency dependence of the real part of the admittance, as given by equation (2.20*a*).

For a finite network of size $N \times N$, the typical spacing between resonances scales as $1/N^2$, as already mentioned in section 4.3. Since two resonances of comparable strengths are resolved, i.e. separately visible, if their spacing is larger than the width $1/Q$ of each of them, we are led to propose the following finite-size scaling law for the fraction of visible resonances

$$\frac{(n_R)_{\mathrm{visib}}}{n_R} \approx F\left(\frac{Q}{N^2}\right). \tag{4.5}$$

The scaling function $F(X)$ is expected to grow monotonically from $F(0) = 0$, since a vanishing fraction of the resonances is visible if Q does not scale as N^2, to $F(\infty) = 1$,

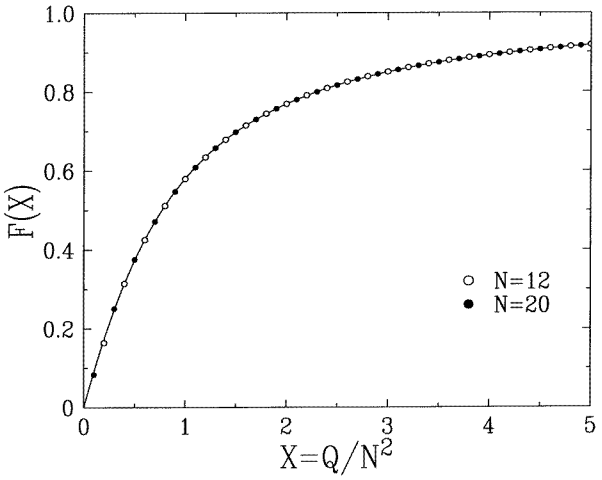

Figure 9. Plot of the finite-size scaling function $F(X)$ of the fraction of visible resonances, against the scaling variable $X = Q/N^2$. Data correspond to samples of size $N \times N$, with $N = 12$ and $N = 20$, at $p = \frac{1}{2}$. The full curve, showing the fit described in the text, is meant as a guide for the eye.

since all the resonances of a finite sample are eventually visible for a large enough quality factor.

Figure 9 shows a plot of the fraction of visible resonances over the whole spectrum ($0 \leqslant \lambda \leqslant 1$), for $p = p_c = \frac{1}{2}$. The observed collapse of the data for the sizes 12×12 and 20×20 clearly demonstrates the validity of the scaling law (4.5). The full curve shows a numerical fit of both series of data to the common analytical form $1/(1 - F(X))^2 = 1 + XP_2(X)$, with $P_2(X)$ being a quadratic polynomial. The quality of the fitted curve, meant as a guide to the eye, suggests a linear behaviour of the scaling function at small X, as well as a power-law convergence of the form

$$1 - F(X) \sim X^{-3/2} \qquad (X \gg 1). \tag{4.6}$$

The fraction of visible resonances depends *a priori* on how uniformly the resonances are distributed, and on the dispersion in the corresponding residues α_a. Both features can depend quantitatively on the concentration p. The scaling function $F(X)$ is therefore expected not to be universal, but rather to weakly depend on the concentration p and on the range of values of λ under consideration. Its main qualitative features, such as the power law (4.6) are, however, expected to be universal. The same remarks apply to the distribution of spacings between resonances, investigated in section 4.3.

4.5. Distribution of local electric fields

The algorithm presented in section 3 also gives access to the spatial structure of the resonances. Indeed, the eigenvector $\boldsymbol{X}_a$ directly provides a map of the electric potentials at the resonance corresponding to the eigenvalue λ_a. For each resonance, we define the local electric field on the bond $(\boldsymbol{x}, \boldsymbol{y})$ as

$$E_{\boldsymbol{x},\boldsymbol{y}} = V_{\boldsymbol{x}} - V_{\boldsymbol{y}} = c((\boldsymbol{X}_a)_{\boldsymbol{x}} - (\boldsymbol{X}_a)_{\boldsymbol{y}}). \tag{4.7}$$

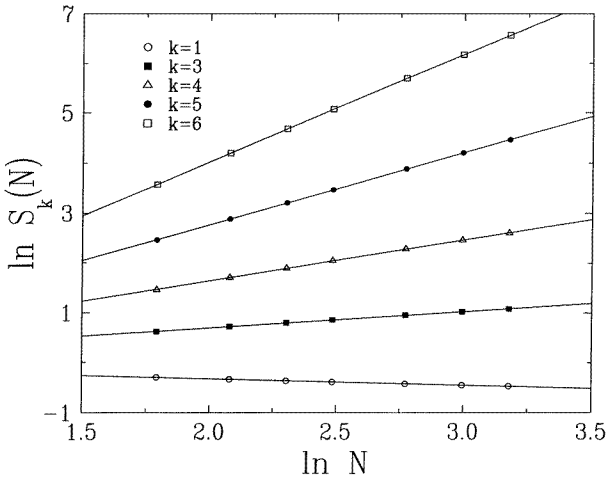

Figure 10. Log–log plot of the moments $S_k(N)$ of the local electric field at resonance, measured in the range (4.3), against the linear sample size N ($6 \leqslant N \leqslant 24$).

The electric fields are defined up to an overall multiplicative constant c. We choose this constant to be $c = \sqrt{n_B}$, so that the normalization (3.19) of the eigenvectors implies

$$\sum_{(x,y)} E_{x,y}^2 = n_B. \tag{4.8}$$

One could think of many ways of analysing the spatial structure of the electric field at resonance. We have chosen to investigate the distribution of the local field living on any given bond. More precisely, we have evaluated the successive moments of this distribution on square samples of size $N \times N$, namely

$$S_k(N) = \langle |E|^k \rangle = \left\langle \frac{1}{n_B} \sum_{(x,y)} |E_{x,y}|^k \right\rangle. \tag{4.9}$$

The normalization (4.8) ensures the identities $S_0(N) = S_2(N) = 1$.

Figure 10 shows a log–log plot of the first non-trivial moments, of index $k = 1$, 3, 4, 5, and 6, against the linear size N of the sample, from $N = 6$–24. Data are obtained in the range (4.3), with around 10^7 random bonds for each sample size. Power laws of the form

$$S_k(N) \sim N^{x_k} \tag{4.10}$$

are clearly apparent. This scaling behaviour, with a non-trivial dependence of the exponent x_k on the index k, is a signature of multifractality [27, 28]. Along the lines of the multifractal formalism, we introduce the generalized (Rényi) dimensions d_k, such that

$$x_k = \frac{(k-2)(2-d_k)}{2}. \tag{4.11}$$

The d_k are expected to decrease from $d_0 = 2$, the dimension of the network, to $d_\infty = 0$.

In physical terms, multifractality implies that the patterns of resonant electric fields exhibit strong local fluctuations, rather similar to those observed in wavefunctions of the Anderson model, in the marginal two-dimensional situation [29]. In particular the resonances are neither localized nor extended, in the conventional sense of these expressions. Indeed, extended patterns of electric fields would correspond to $d_k = 2$ for all $k \geqslant 0$, while localized ones would have $d_k = 0$ for $k \geqslant 1$. We recall that a similar phenomenon of multifractality

Table 2. Exponents x_k and associated generalized dimensions d_k characterizing the multifractal distribution of local electric fields at resonance, measured in the range (4.3).

k	Exponent x_k	Dimension d_k
0	0	2
1	-0.097 ± 0.016	1.806 ± 0.032
2	0	—
3	0.295 ± 0.018	1.410 ± 0.036
4	0.769 ± 0.026	1.231 ± 0.026
5	1.390 ± 0.026	1.074 ± 0.018
6	2.130 ± 0.024	0.935 ± 0.012

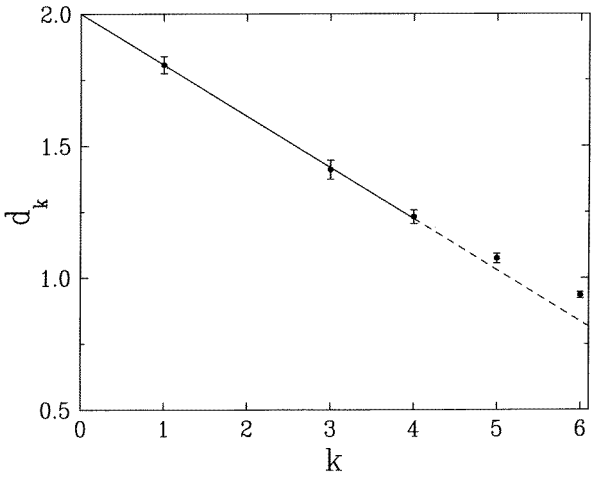

Figure 11. Plot of the generalized dimensions d_k of the distribution of electric fields at resonance, measured in the range (4.3), against index k. The straight line shows the linear behaviour (4.12), with $\beta = 0.194$.

has been reported for the DC problem of the conductor–insulator mixture, right at the percolation threshold [30, 31].

From a quantitative viewpoint, a more refined fit of the data to the power laws (4.10), including a relative correction in $1/N$, yields more accurate estimates for the exponents x_k and the associated dimensions d_k, listed in table 2. Figure 11 shows a plot of the d_k against the index k. An approximate linear decay of the form

$$d_k \approx 2 - \beta k \tag{4.12}$$

with $\beta \approx 0.194$, is observed over a fairly broad range ($0 \leqslant k \leqslant 4$). A similar linear behaviour has been predicted analytically for the two-dimensional Anderson model in the weak-disorder regime [29]. The linear law (4.12) corresponds to a log-normal (LN) distribution of the local fields. Indeed, let us set

$$\ell = \ln |E|. \tag{4.13}$$

The scaling law (4.10) then reads $\langle \exp(k\ell) \rangle \sim \exp(Bk(k-2)/2)$, with $B = \beta \ln N$. Neglecting the k-dependence of the prefactor, this last expression corresponds to a LN

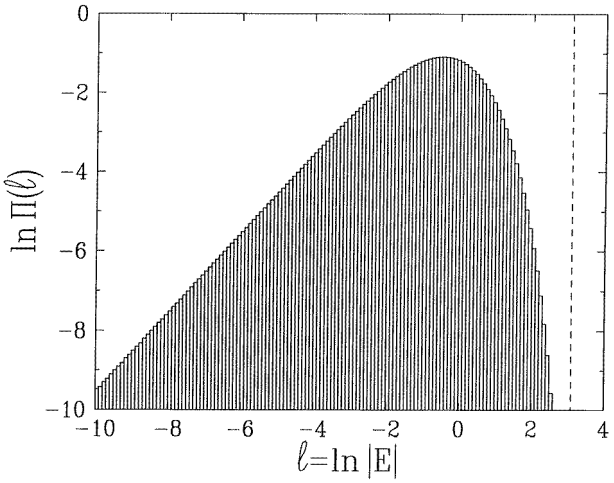

Figure 12. Logarithmic histogram plot of the probability density $\Pi(\ell)$ of $\ell = \ln|E|$, the logarithm of the electric field at resonance, for samples of size 16×16, measured in the range (4.3). The broken vertical marks the upper bound $\ell_{\max} = (\ln n_B)/2$, with $n_B = 481$.

distribution for $|E|$, i.e. to a Gaussian law for the logarithmic variable ℓ, namely

$$\Pi_{\mathrm{LN}}(\ell) = (2\pi B)^{-1/2} \exp\left(-\frac{(\ell + B)^2}{2B}\right). \tag{4.14}$$

The actual probability density $\Pi(\ell)$ is shown in figure 12, for networks of size 16×16 in the range (4.3). This very asymmetric distribution looks quite different from a LN law. In particular, it falls off as $\Pi(\ell) \sim \exp(-\ell)$ as $\ell \to -\infty$, yielding a finite value at $|E| = 0$ of the probability density $P(|E|) = e^{\ell}\Pi(\ell)$. Most of the dependence of the distribution on the sample size N takes place to the right of the plot, for large values of ℓ, close to the upper bound $\ell_{\max} = (\ln n_B)/2$, where a very fast decay is observed.

5. Discussion

We have investigated the AC conductivity of binary random networks of complex impedances, with emphasis on its analytic structure in the complex variable h or λ, and on the corresponding resonant behaviour. The present analysis is an extension to the general binary case of a previous work [2], devoted to the resonant response of a finite cluster, or set of clusters, embedded in an infinite homogeneous host lattice. Along the lines of [1, 2], the poles of the conductance are interpreted in terms of the resonances which show up in the AC conductivity of the $RL - C$ model, and of the relaxation times in the transient response of the $R - C$ model. We have proposed an efficient algorithm, which allows the determination of the rational λ-dependence of the conductance Y of a finite sample, in terms of its poles λ_a and of the associated residues α_a. A very similar formalism had been proposed long ago by Straley [6].

We wish to underline again that the main advantage of this approach is to give at once the analytic structure of the conductance in h or λ, for any finite sample. As far as a numerical investigation of the resonant response is concerned, this approach is therefore more suitable than the usual numerical methods, which can only yield the conductivity of the binary model for a fixed value of the ratio h, such as the transfer-matrix method [12], or

the iterative algorithm based on the $Y-\Delta$ transformation [32], used for example in [7]. It is also worth noting that our approach yields the full analytic structure of the conductance, including the static conductance of the $\mathcal{Q}$-phase of any finite sample. Indeed the latter quantity is given by equation (2.3), with the corresponding residue α_1 being given by the sum rule (2.5) in terms of all the other residues, corresponding to genuine resonances.

An extensive use of this algorithm, in the case of the square lattice, has allowed us to investigate in detail many aspects of the resonant dielectric response of the binary model. In general we have used 10^7 random bonds or more per measurement, a good enough statistics to obtain very accurate data. We have investigated the density of resonances $\rho(p,x)$ and the spectral function $H(p,x)$. This approach yields a better evaluation of the spectral function than the more direct method, consisting of measuring the imaginary part of the conductivity. The most salient structures have been labelled, at least for a small enough concentration p, by resonances of configurations made of one to three bonds, which can be determined exactly, along the lines of [2]. The data for the spectral function have also been compared with the EMA prediction.

The Lifshitz behaviour of the density of resonances near the endpoints has been successfully characterized. A good qualitative agreement is found with the argument of Hesselbo [21], according to whom the analogues of the Lifshitz sphere are linear extended objects, such as hairpins. From a quantitative viewpoint, our data suggest that other classes of extended structures may also contribute to the Lifshitz tails, even for a small concentration p. The present situation is a lucky one, since numerical investigation of Lifshitz tails in more than one dimension is known to be a very difficult task in general, especially in the case of binary disorder [20]. The distribution of the spacings between neighbouring resonances has been found to be in qualitative agreement with the universal distribution of the GOE universality class of random matrices, although small but definite differences show up at a quantitative level. The number of visible resonances of the $RL-C$ model on a finite sample of size $N\times N$, as a function of the quality factor Q, has been shown to obey a finite-size scaling law (4.5), involving a scaling function $F(X)$ of the variable $X=Q/N^2$. Quantities such as the scaling function $F(X)$, or the spacing distribution $P(s)$, are expected not to be universal: quantitative features of these functions should rather weakly depend on the concentration p and on the range of resonances considered, the range (4.3) being meant as a generic example.

More generally, for the binary model on a d-dimensional lattice, the appropriate finite-size scaling variable describing dielectric resonances reads $X=Q/N^d$. Indeed, the number of resonances on a sample of linear size N scales as its volume N^d. This observation yields in particular a prediction for the divergence of the current correlation length ξ in the weak-dissipation regime ($Q\gg 1$). By setting $X\sim 1$ for $N\sim\xi$, we obtain

$$\xi\sim Q^{\bar{\nu}} \qquad \text{with } \bar{\nu}=\frac{1}{d}. \tag{5.1}$$

We thus recover a simple result due to Hesselbo [21], which has been corroborated by numerical simulations, yielding $\bar{\nu}=0.4\pm 0.1$ in two dimensions [8].

Finally, we have investigated the distribution of the resonant electric field living on any given bond. The moments of this distribution obey power laws with non-trivial exponents x_k, a characteristic feature of multifractality. The associated generalized dimensions d_k are found to behave similarly to those observed in the Anderson model of localization, in the marginal two-dimensional case [29]. Multifractality thus appears to be a quite generic feature of the resonant response of binary networks. In particular, this phenomenon is unrelated to the percolation transition. In analogy with the fraction of visible resonances or

the spacing distribution $P(s)$, the exponents x_k and the dimensions d_k are expected not to be fully universal, but to exhibit a weak dependence on the concentration p, and possibly on the range of resonances considered.

This multifractal picture provides a quantitative characterization of local features of the fluctuations in electric fields at resonance observed previously [8]. These giant fluctuations have been argued to be responsible for surface-enhanced Raman scattering, this phenomenon being especially pronounced in strongly disordered semicontinuous films. There is a regime where the enhancement factor is predicted to be proportional to $\langle E^4 \rangle$ [9], whence the relevance of the dimension d_4, in our notation. In a realistic system, with a small but finite dissipation rate $1/Q$, these fluctuations are expected to be critical, i.e. to exhibit strong spatial correlations, on scales smaller than the current correlation length ξ, estimated in equation (5.1). Since the algorithm used in this work gives direct access to the full map of electric fields at resonance, it could be used to investigate other aspects of dielectric resonances, including their spatial correlations, on which some information is already available [8].

Acknowledgments

It is a pleasure for us to thank F Brouers, J P Clerc, G Giraud and L Raymond for fruitful discussions, and M F Thorpe for an interesting correspondence. Part of this work has been done by ThJ during his *Stage de DEA de Physique Quantique* (Paris).

References

[1] Clerc J P, Giraud G, Laugier J M and Luck J M 1990 *Adv. Phys.* **39** 191
[2] Clerc J P, Giraud G, Luck J M and Robin Th 1996 *J. Phys. A: Math. Gen.* **29** 4781
[3] Brouers F, Clerc J P and Giraud G 1991 *Phys. Rev.* B **44** 5299
Brouers F, Clerc J P, Giraud G, Laugier J M and Randriamanantany Z A 1993 *Phys. Rev.* B **47** 666
Brouers F, Jolet J M, Giraud G, Laugier J M and Randriamanantany Z A 1994 *Physica* **207A** 100 and references therein
[4] Bergman D J 1978 *Phys. Rep.* **43** 377
Bergman D J 1980 *Phys. Rev. Lett.* **44** 1285
Bergman D J 1981 *Phys. Rev.* B **23** 3058
Bergman D J 1982 *Ann. Phys.* **138** 78
[5] Milton G W 1980 *Appl. Phys. Lett.* **37** 300
Milton G W 1981 *J. Appl. Phys.* **52** 5286
Milton G W 1981 *J. Appl. Phys.* **52** 5294
Milton G W 1981 *Phys. Rev. Lett.* **46** 542
[6] Straley J P 1979 *J. Phys. C: Solid State Phys.* **12** 2143
[7] Day A R and Thorpe M F 1996 *J. Phys.: Condens. Matter* **8** 4389
[8] Brouers F, Blacher S and Sarychev A K 1995 *Fractals in the Natural and Applied Sciences* ed N M Novak (London: Chapman and Hall) p 237
[9] Brouers F, Blacher S, Lagarkov A N, Sarychev A K, Gadenne P and Shalaev V M 1997 *Phys. Rev.* B **55** 13 234
Gadenne P, Brouers F, Shalaev V M and Sarychev A K 1998 *J. Opt. Soc. Am.* B **15** 68
[10] Kramers H A and Wannier G H 1941 *Phys. Rev.* **60** 252
[11] Straley J P 1977 *Phys. Rev.* B **15** 5733
[12] Normand J M, Herrmann H J and Hajjar M 1988 *J. Stat. Phys.* **52** 441
[13] Luck J M 1991 *Phys. Rev.* B **43** 3933
[14] Bruggeman D A G 1935 *Ann. Phys., Lpz.* **24** 636
[15] Landauer R 1952 *J. Appl. Phys.* **23** 779
[16] Kirkpatrick S 1973 *Rev. Mod. Phys.* **45** 574
[17] Mochán W L and Barrera R G 1994 *Proc. ETOPIM 3 Physica* **207A** 1–462

Dykhne A M, Lagarkov A N and Sarychev A K 1997 *Proc. ETOPIM 4 Physica* **241A** 1–452
[18] Lifshitz I M 1964 *Adv. Phys.* **13** 483
Lifshitz I M 1965 *Sov. Phys.–Usp.* **7** 549
[19] Nieuwenhuizen Th M 1990 *Physica* **167A** 43
[20] van Rossum M C W, Nieuwenhuizen Th M, Hofstetter E and Schreiber M 1994 *Phys. Rev.* B **49** 13 377
[21] Hesselbo B 1994 *DPhil Thesis* (Oxford)
[22] Stauffer D and Aharony A 1992 *Introduction to Percolation Theory* 2nd edn (London: Taylor and Francis)
[23] Ziff R M, Finch S R and Adamchik V S 1997 *Phys. Rev. Lett.* **79** 3447
[24] Watts M G 1975 *J. Phys. A: Math. Gen.* **8** 61
[25] Bohigas O 1991 *Chaos and Quantum Physics, Les Houches, Session LII* ed M J Giannoni, A Voros and J Zinn-Justin (Amsterdam: North-Holland)
[26] Mehta M L 1967 *Random Matrices and Statistical Theory of Energy Levels* (London: Academic) new revised and enlarged edition 1990
[27] Paladin G and Vulpiani A 1987 *Phys. Rep.* **156** 147
[28] Feder J 1988 *Fractals* (New York: Plenum)
[29] Fal'ko V I and Efetov K B 1995 *Europhys. Lett.* **32** 627
Fal'ko V I and Efetov K B 1995 *Phys. Rev.* B **52** 17 413 and references therein
[30] Rammal R, Tannous C, Breton P and Tremblay A-M S 1985 *Phys. Rev. Lett.* **54** 1718
Rammal R, Tannous C and Tremblay A-M S 1985 *Phys. Rev.* A **31** 2662
[31] de Arcangelis L, Redner S and Coniglio A 1985 *Phys. Rev.* B **31** 4725
[32] Lobb C J and Franck D J 1984 *Phys. Rev.* B **30** 4090
Franck D J and Lobb C J 1988 *Phys. Rev.* B **37** 302